Ore Geology Reviews 112 (2019) 103019

Contents lists available at ScienceDirect

Ore Geology Reviews

journal homepage: www.elsevier.com/locate/oregeorev

# Trace elemental modification in magnetite from high-grade metamorphosed BIFs in the southern North China Craton

Caiyun Lan[a], Taiping Zhao[b,*], Wei Terry Chen[c], Xiaoping Long[a]

[a] State Key Laboratory of Continental Dynamics, Department of Geology, Northwest University, Xi'an 710069, China
[b] Key Laboratory of Mineralogy and Metallogeny, Guangzhou Institute of Geochemistry, Chinese Academy of Sciences, Guangzhou 510640, China
[c] State Key Laboratory of Ore Deposit Geochemistry, Institute of Geochemistry, Chinese Academy of Sciences, 550002 Guiyang, China

ARTICLE INFO

*Keywords:*
Magnetite
Trace element composition
LA-ICP-MS
Metamorphism
Banded iron formations
North China Craton

ABSTRACT

Magnetite, as a common oxide mineral in banded iron formations (BIFs) and ore deposits, is an ideal provenance indicator for mineral exploration, and its composition has long been used for genetic studies of ore deposits. However, many ore deposits, particularly the BIFs worldwide, have undergone various grades of secondary metamorphism or hydrothermal alteration. It is still unclear whether the original magnetite composition was modified during the secondary processes and, if so, to what extent the compositions were modified. In this study, we conduct mineralogical and LA-ICP-MS trace elemental investigations on magnetite from the amphibolite- to granulite-facies metamorphosed BIFs in the southern North China Craton. The new results were compared with those of unmetamorphosed and greenschist-facies metamorphosed BIFs worldwide to understand how the original composition of magnetite was modified during different grades of metamorphism. Magnetite grains from the amphibolite- to granulite-facies BIFs have low Cr, Co, Ni and Ga (less than 10 ppm) and slightly variable V and Zn. These elements do not show remarkable changes during high-grade metamorphism when compared with the unmetamorphosed and greenschist-facies metamorphosed magnetite, indicating that these elements in magnetite are immobile during metamorphism. A very narrow range of $Fe^{2+}/Fe^{3+}$ mole ratios of the high-grade metamorphosed magnetite roughly suggest limited changes of oxygen fugacity during metamorphism, which is also supported by the limited change of Cr and V contents. High Mn contents in these magnetite grains are associated with low Mg contents possibly due to the fact that these elements occupy the same site in magnetite structure. Compared with unmetamorphosed magnetite, the high-grade metamorphic magnetite in the BIFs of the southern North China Craton has elevated Al, Ti and Mn. Such a change of magnetite compositions is mainly controlled by coexisting Fe-Mg silicates that formed during high-grade metamorphism. For example, our new results of trace elemental mapping on magnetite show that the edge of magnetite grains that are in contact with Fe-Mg silicates (e.g., hornblende, grunerite and pyroxene) are remarkably enriched in Mg, Mn, Al, Si, and Na compared to the cores (some elements up to 10 times more). All these features indicate that elemental diffusion and exchange between magnetite and coexisting silicate minerals during high-grade metamorphism have extensively modified original compositions of magnetite from BIFs.

## 1. Introduction

Banded iron formations (BIFs) are iron-rich (15–40 wt% Fe) and siliceous (40–60 wt% $SiO_2$) chemical sedimentary rocks that precipitated from seawater throughout the Precambrian Eon (James, 1954; Gross, 1980). The amount of preserved BIFs on the present-day Earth is estimated to be about $10^{14\text{-}15}$ tons (Isley, 1995), and BIFs are the principle source of iron for the global steel industry, giving their greatly economic importance (Bekker et al., 2010). Magnetite, as an abundant and widespread oxide mineral in BIFs and other hydrothermal deposits, is an ideal provenance indicator for mineral exploration and useful for genetic studies of ore deposits (Grigsby, 1990; Dupuis and Beaudoin, 2011; Dare et al., 2012; Nadoll et al., 2014). However, most worldwide BIFs and other types of deposits have undergone various grades of metamorphosed alteration in later-stage. Therefore, clearly understanding how the primary chemistry of magnetite has been modified is important for precisely interpreting its compositional data, particularly when they are used for provenance discrimination.

Magnetite belongs to the space group Fd3m and has an inverse spinel structure with the general stoichiometry of $(Fe^{2+})(Fe^{3+})_2O_4$

* Corresponding author.
*E-mail address:* tpzhao@gig.ac.cn (T. Zhao).

https://doi.org/10.1016/j.oregeorev.2019.103019
Received 2 February 2019; Received in revised form 9 May 2019; Accepted 14 July 2019
Available online 16 July 2019

(Bragg, 1915; Lindsley, 1976; Fleet, 1981; Wechsler et al., 1984). Some trace elements can partially exchange with Fe in this structure and occupy its site (e.g., Mg, Ni, Mn, Co, or Zn, which have a 2+ charge, and Al, Cr, V, Mn, or Ga, which have a 3+ charge, can exchange with $Fe^{2+}$ and $Fe^{3+}$, respectively. Titanium, which has a 4+ charge, can also occupy the $Fe^{3+}$ site when substitution is coupled with a divalent cation (Wechsler et al., 1984)), leading to different genetic magnetite with characteristic trace elemental concentrations (Dupuis and Beaudoin, 2011; Dare et al., 2012; Nadoll et al., 2014). However, magnetite geochemistry always records a mixed information as secondary alteration overprint. Numerous studies regarding the controlling factors (e.g., temperature, pressure, cooling rate, oxygen or sulfur fugacity) of these trace elemental concentrations in magnetite are mostly available for igneous magnetite (e.g., Buddington and Lindsley, 1964; Frost and Lindsley, 1991; Mollo et al., 2013). Recently, based on this, some studies discussed similar factors controlling the chemical modification of magnetite formed in hydrothermal processes by comparing different types of ore deposits (e.g., Nadoll et al., 2014; Chen et al, 2015). Besides, some studies have tentatively considered that the composition of metamorphic magnetite is likely controlled by temperature ($T$) (Frost, 1991), oxygen fugacity ($fO_2$) (Frost, 1991) and metamorphic grade (Evans and Frost, 1975; Van Baalen, 1993; Skublov and Drugova, 2003), but such interpretations have not been convincingly confirmed, partially due to the lack of sufficient compositional data for variably metamorphosed magnetite. More importantly, the mechanism of these factors controlling is still not clear.

Most Archean to early Paleoproterozoic BIFs have undergone various grades of metamorphism with metamorphic temperature ranging from 200 °C to 800 °C after diagenesis (French, 1968; Bonnichsen, 1969; Klein, 1978; Konhauser et al., 2017). This temperature range is similar to the ore-forming temperature of other important hydrothermal deposits, such as, 300 °C to 800 °C for porphyry ore deposit and 300 °C to 500 °C for skarn ore deposit (Ahmad and Rose, 1980; Sillitoe, 2010). Mass of metamorphic reactions or recrystallization are happened between gangue minerals in BIFs under special conditions during such high-grade metamorphism, leading to the formation of new Fe-rich silicates (e.g., minnesotaite, amphiboles, pyroxenes, and fayalite) and metamorphic fluids (Klein, 2005). Most of these Fe-rich silicates are enriched in Mg, Al and Ti, which likely affect the compositions of magnetite during metamorphosed reactions (Skublov and Drugova, 2003). Notably, post-diagenesis metamorphic processes in BIFs are essentially isochemical except for prevalent dehydration and decarbonation and no other external factors need to be considered (Klein, 2005). Therefore, magnetite geochemistry from variable metamorphosed BIFs can help to investigate the controlling factors and their mechanism.

In this study, we conducted mineralogical and trace elemental investigations on the metamorphosed BIFs in the Xuchang, Xincai and Wuyang areas, which is located on the southern margin of the North China Craton (NCC) (Fig. 1). The Xuchang and Xincai BIFs have undergone amphibole-facies metamorphism whereas the Wuyang BIF has undergone granulite-facies metamorphism with metamorphic temperatures ranging from 650 °C to 810 °C (Qi and Yao, 1982; Qi, 1987; Lu et al., 2013, 2014; Lan, 2015). These metamorphic BIFs are characterized by different assemblage of Fe-rich silicates including amphibole and biotite in amphibole-facies BIFs and clinopyroxene and orthopyroxene in granulite-facies BIF, thus providing a good opportunity to examine the possible modifications of magnetite chemistry during variable degrees of metamorphism. We obtained major elements of magnetite by electron probe microanalyzer (EPMA) and trace elemental compositions and elemental mapping of magnetite by laser ablation inductively coupled plasma mass spectrometry (LA-ICP-MS). The new dataset, in combination with previously published compositional data for magnetite in unmetamorphosed and low-grade metamorphic BIFs worldwide, allows us to discussed the compositional changes of variable grade metamorphosed magnetite and extent to which the chemistry of magnetite is modified under different metamorphic grades.

## 2. Geologic setting

### 2.1. Regional geology

The NCC is one of the oldest cratons in the world and hosts a large number of Paleoproterozoic to Archean BIFs (Liu et al., 1992; Zhang et al., 2012). The basement of the NCC is mainly composed of Archean to Paleoproterozoic tonalite-trondhjemite-granodiorite (TTG) gneisses, meta-volcanic and sedimentary rocks, and sparse Paleoarchean and Mesoarchean rocks (> 3400 Ma) (Jahn and Ernst, 1990; Zhao et al., 2001); it is overlain by Mesoproterozoic to Phanerozoic unmetamorphosed sedimentary rocks (Jahn and Ernst, 1990). The NCC was formed by the assembly of several micro-continental blocks (Zhao et al., 2001; Zhai et al., 2005; Zhai and Santosh, 2011), and the continental crust of the NCC was largely formed by the end of the Neoarchean (ca. 2.5 Ga) (Zhai and Liu, 2003), with two periods of crustal growth occurring from 2.8 to 2.7 Ga and 2.6–2.5 Ga (Zhai et al., 2005; Zhai and Santosh, 2011). Subsequently, the NCC underwent Paleoproterozoic multi-stage rifting and collision to form a uniform block ca. 1.85 Ga (Kusky et al., 2001; Zhai and Liu, 2003; Zhao et al., 2005; Santosh et al., 2009), leading to corresponding multi-stage metamorphism overprint.

The Dengfeng, Taihua and Huoqiu complexes are the most widely exposed Paleoproterozoic to Archean basement rocks in the southern margin of the NCC (Fig. 1). These complexes comprise similarly two distinct lithologic units including plutonic rocks and supracrustal assemblage. The plutonic rocks are composed of TTG gneisses and granites. The supracrustal assemblages of the Dengfeng, Taihua and Huoqiu complexes, which are named as the Dengfeng Group, Taihua Group and Huoqiu Group, respectively, are successions of metamorphosed volcano-sedimentary rocks. The Dengfeng Group consists of mylonitic metavolcanic rocks, biotite-hornblende gneisses, hornblende schists, BIFs and garnet-biotite-quartz schists, and is subdivided into the Caomiaozhang, Wuzhuang and Huayang formations (HBGMR, 1989). The mineral assemblages of garnet, staurolite, biotite and quartz indicate that the Dengfeng Group has underwent amphibolite-facies metamorphism. Metamorphosed volcanic rocks in the different formations of the Dengfeng Group have given similar zircon U-Pb ages between 2540 and 2508 Ma (Kröner et al., 1988; Wan et al., 2009; Diwu et al., 2011). Meta-mafic volcanic rocks in the Dengfeng Group have geochemical features similar to MORB and island arc tholeiites, which is interpreted to have erupted in a back-arc basin (Zhou et al., 2009).

The Taihua group has been tentatively subdivided into the Neoarchean lower Taihua Group and Paleoproterozoic upper Taihua Group based on rock types and ages (Zhang et al., 1985; Kröner et al., 1988; Xue et al., 1995; Tu, 1998; Wan et al., 2006; Yang, 2008). The lower Taihua Group, which underlies the upper Taihua Group, is mainly composed of meta-mafic rocks that occur as enclaves of, commonly less than 100 m in length in the widely distributed TTG rocks (Zhang et al., 1985; Kröner et al., 1988). The upper Taihua Group, exposed mainly in the Tongguan, Luoning, Lushan and Wuyang areas (Fig. 1), has thickness of several kilometers and is composed of metapelites, meta-arenites, BIFs, meta-carbonates, carbonaceous metamorphic rocks and meta-mafic rocks (Shen, 1994; Xue et al., 1995; Tu, 1998; Wan et al., 2006). The upper Taihua Group has variable lithology assemblages and was subdivided into different formations in different location. For example, the upper Taihua Group in the Wuyang area was subdivided into the Zhaoanzhuang, Tieshanmiao and Yangshuwan formations (Liang et al., 1981; Yu et al., 1981, 1982, 1983). Based on their distribution, mineral assemblages and composition, the protoliths of the rocks in this area represent a suite of sequences containing mafic volcanic rocks, chemical sedimentary rocks, pelites, arenites and carbonaceous clastic rocks that were deposited in a back-arc basin (Lan et al., 2017). The Taihua group in the Wuyang area has undergone multiple amphibolite- to granulite-facies metamorphic events (e.g., 1.96 Ga, 1.85 Ga; $T$ = 650–810 °C, $P$ = 4.9–10.8 kbar, Lu et al., 2013,

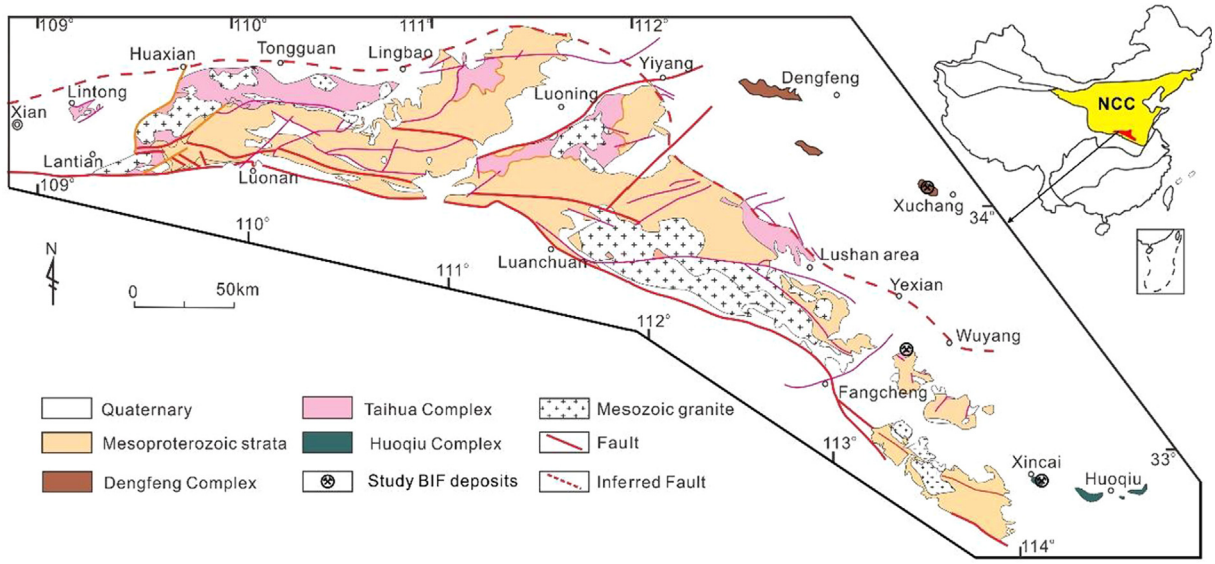


**Fig. 1.** Geological distribution of the exposed Archean to Paleoproterozoic basement including Dengfeng, Taihua and Huoqiu complexes in the southern margin of the North China Craton (NCC), and the location of the study BIF deposits in this paper (modified after Diwu et al., 2014).

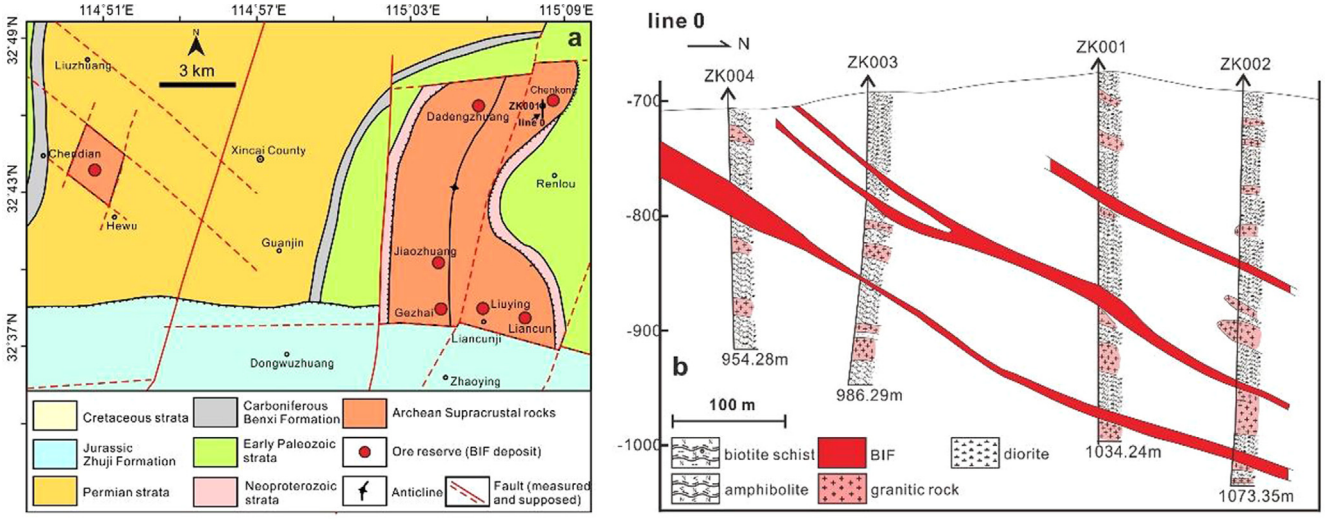


**Fig. 2.** (a) Geological map of Neoarchean supracrustal rocks in the Xincai area showing the distribution of the Xincai BIF and exploration line 0 (modified after GIIHP, 2008). (b) Cross-section profile of line 0 showing distribution of the Xincai BIF and associated rocks (modified after GIIHP, 2008).

2014) and complex tectonic deformation.

The Huoqiu Group can be divided into three formations due to poor outcrop in the field. According to the rock association and information from drill core, the geological framework of this region is mostly inferred through available information from lithological association and drill-core data. Thus, the lower units comprise the Huayang and the Wuji formations which are conformably overlain by the upper Zhouji Formation. The Huoqiu group predominantly consists of the Neoarchean metasedimentary rocks, marbles, amphibolites and BIFs in the Huoqiu area (Qi and Yao, 1982; Wan et al., 2010). The Huoqiu Group has undergone multiple amphibolite-facies metamorphic events including 2.7 Ga (Yang et al., 2012) and 1.84 Ga (Wan et al., 2010) with metamorphic conditions of 650 to 750 °C and 5.5 ± 0.5 kbar (Qi and Yao, 1982; Qi, 1987). The Huoqiu Group has formed in a sea basin on a continental margin based on multiple facies (carbonate, oxide and silicate facies) of therein BIF (Huang, 2014; Huang et al., 2016; Liu and Yang, 2015).

### 2.2. The Xuchang BIF

The ~2.54 Ga Xuchang BIF (Kröner et al., 1988; Wan et al., 2009; Diwu et al., 2011) is hosted in the Wuzhuang Formation of the Dengfeng Group, which was completely covered by Quaternary sediments. Strata associated with the Xuchang BIF consist mainly of amphibolite and plagioclase-biotite leptynite. Drilling revealed that the ore body in this area is 150 to 300 m underground and more than 10 to 50 m thick. Multiple BIF layers of the ore bodies extend steadily along the strike of the strata, and they have variable thickness ranging from a few meters to fifty meters. Each of the ore body is 45° SW dipping and is composed of Fe ores with 1 to 6 layers, each of which has an average thickness of up to ~10 m. Ore types of the Xuchang BIF are dominated by banded quartz-amphibole-magnetite ore, which is composed of magnetite, amphibole, minor grunerite and biotite. The Fe-rich bands are composed of magnetite, amphibole and minor biotite and quartz. Magnetite grains in the Fe-rich bands are either dispersed in the amphibole matrix or therein as inclusions, whereas the Si-rich bands are composed of quartz and minor amphibole and biotite.

### 2.3. The Xincai BIF

The 2.5–2.7 Ga (Lan et al., 2019) Xincai BIF located in Xincai County that is 70 km west of the Huoqiu BIFs along the NW-SE trending BIF-bearing supracrustal belt (Fig. 1) (Cui et al., 2008). The BIF-bearing supracrustal rocks in the Xincai area were completely covered by Neoproterozoic strata and Quaternary sediments (Fig. 2). Drilling revealed that the supracrustal rocks in this area are 700 m underground and more than 300 m thick (Fig. 2b). Strata associated with the Xincai BIF consist mainly of amphibolite, BIF and biotite schist (Fig. 2b). Mineral assemblages of amphibole-garnet-biotite in the biotite schist generally reflect amphibolite-facies regional metamorphism. A series of ore clusters can be observed in Chenkong, Dadengzhuang, Jiaozhuang, Gezhai, Liuying and Liancun in eastern Xincai County and Chendian and Hewu in western Xincai County (Fig. 2a). From the drilled section (Fig. 2b), multiple BIF layers of the eastern BIF bodies extend steadily along the strike of the strata, and they have variable thickness ranging from a few meters to tens of meters. The Xincai BIF comprises alternating Fe-rich and Si-rich bands, ranging from < 1 mm to 5 mm in thickness. On the basis of their biotite and grunerite contents, the Xincai BIF can be classified as Type I with abundant biotite and grunerite and Type II with minor biotite and grunerite. The Fe-rich bands of Type I BIF are composed of magnetite and biotite, grunerite and minor quartz (Fig. 3c and d), whereas the Fe-rich bands of Type II BIF are composed of magnetite and minor biotite and grunerite (Fig. 3a and b). Minor pale green to pale brown grunerites occur in the Fe-rich bands (Fig. 3). Single magnetite grains in the Fe-rich bands vary from < 10 μm to 0.5 mm in length (Fig. 3). The Si-rich bands in both type of ores are composed of quartz, minor grunerite and magnetite (Fig. 3b and d). Quartz grains in the Si-rich bands range from microcrystalline (< 10 μm) to 1 mm in diameter, are interlocking, frequently display optical wave extinction and contain small magnetite inclusions (Fig. 3b and d).

### 2.4. The Wuyang BIF

The 2.47–2.15 Ga (Lan et al., 2017) Wuyang BIF is hosted in the Tieshanmiao Formation, which has a NW-trending strike, and is ~14 km long and extends from Shangmiao to Hewan villages (Fig. 4a). The Wuyang BIF in the Shangmiao-Jingshansi-Lenggang mine occurs in the core of a NW-trending regional-scale anticlinorium. The ore bodies, which are 5–83 m thick, are variably dipping and composed of Fe ores with multiple layers (2 to 12 layers), each of which has an average thickness of up to ~6 m. On the other hand, the BIF in the Tiegukeng-Tieshanmiao-Hewan mine (Fig. 4b) occurs in the southern limb of the anticlinorium and has undergone strong deformation related to folding (Fig. 5a and b). In this mine, the ore body is 27–49° SW dipping (Fig. 4b) and is composed of Fe ores with 1 to 3 layers, each of which has an average thickness of up to ~10 m. The bands of the metamorphic BIF are broadly parallel to the schistosity of the interlayers of biotite-plagioclase gneiss (Fig. 5b and f). Two types of iron ores can be identified based on their macro- and micro-textures: banded quartz-pyroxene-magnetite ores (BPM, Fig. 5d–f) and disseminated pyroxene-magnetite ores (DPM, Fig. 5d–f). The DPM ores are present either as lenses within the BPM ores (Fig. 5d) or as bands that are sharply parallel to the BPM ores (Fig. 5e).

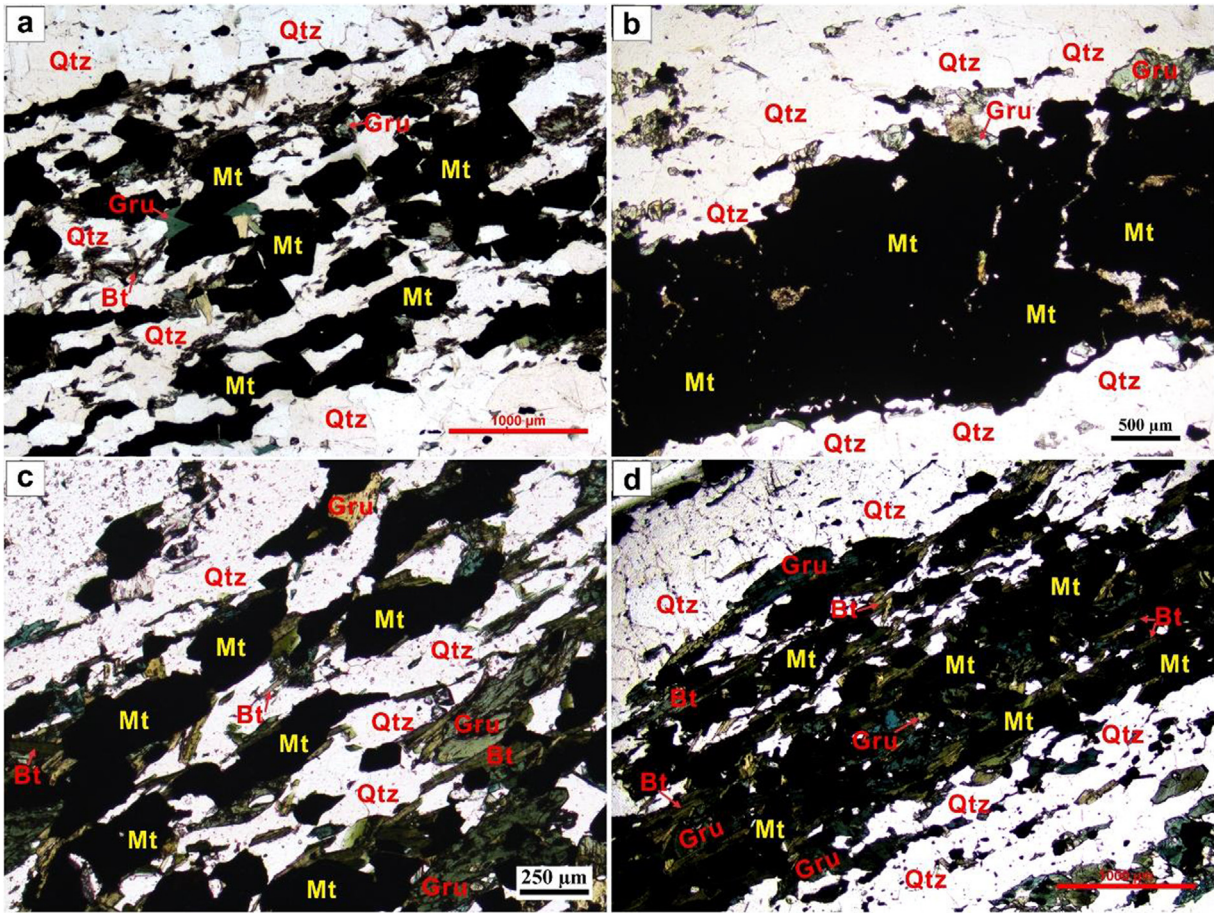


**Fig. 3.** Photographs of the Xincai BIF in the Xincai area showing the mineralogy and typical textures. BIF sample which is composed of Fe-rich and Si-rich bands (plane-polarized light). (a) Variable quartz, grunerite and biotite in Fe-rich band. (b) Minor quartz and grunerite in Fe-rich band. (c) and (d) Abundant biotites and grunerites in Fe-rich band. Qtz-quartz; Gru-grunerite; Bt-biotite; Mt-magnetite.

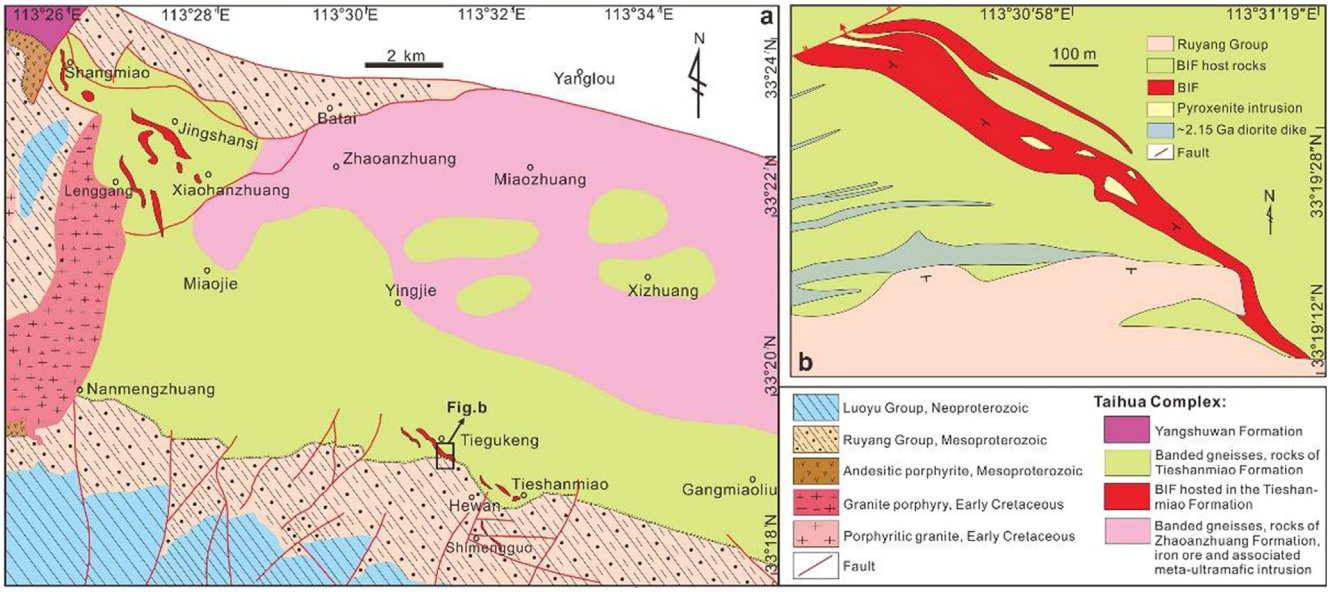


**Fig. 4.** Geological distribution of the exposed Taihua Complex in the Wuyang area (modified after WUSTEEL, 2003): (a) Geological map showing distribution of the Taihua Complex, overlain Mesoproterozoic and Neoproterozoic strata. (b) Geological map of the Wuyang BIF in the Tiegukeng-Tieshanmiao-Hewan (TTH) mining field showing distribution of the BIF and pyroxenite intrusions.

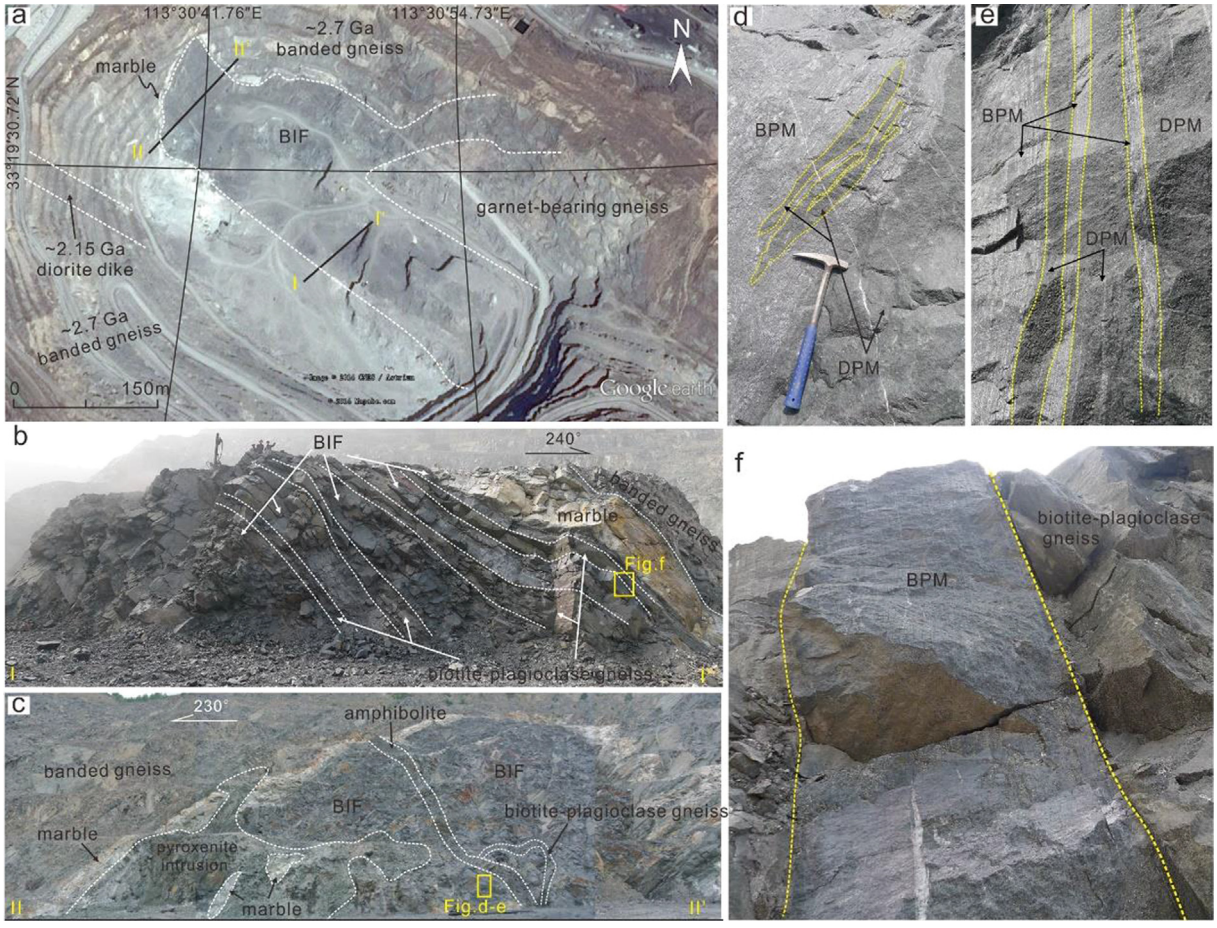


**Fig. 5.** Field relationships of different type rocks. (a) Tiegukeng open pit in the Wuyang area from Google Earth (2014) showing the Wuyang BIF, wall rocks and cross-sections I-I′ and II-II′. (b) Cross-section I-I′ showing interlayers of the BIF rocks and biotite-plagioclase gneiss. (c) Cross-section II-II' showing an intrusion of 2–10 m thick pyroxenite stretches into the BIF body locally. (d-e) Contact relationship of the banded quartz-pyroxene-magnetite ore (BPM) and disseminated pyroxene-magnetite ores (DPM) from cross-section II-II'. (f) Contact relationship of the BPM and biotite-plagioclase gneiss rocks.

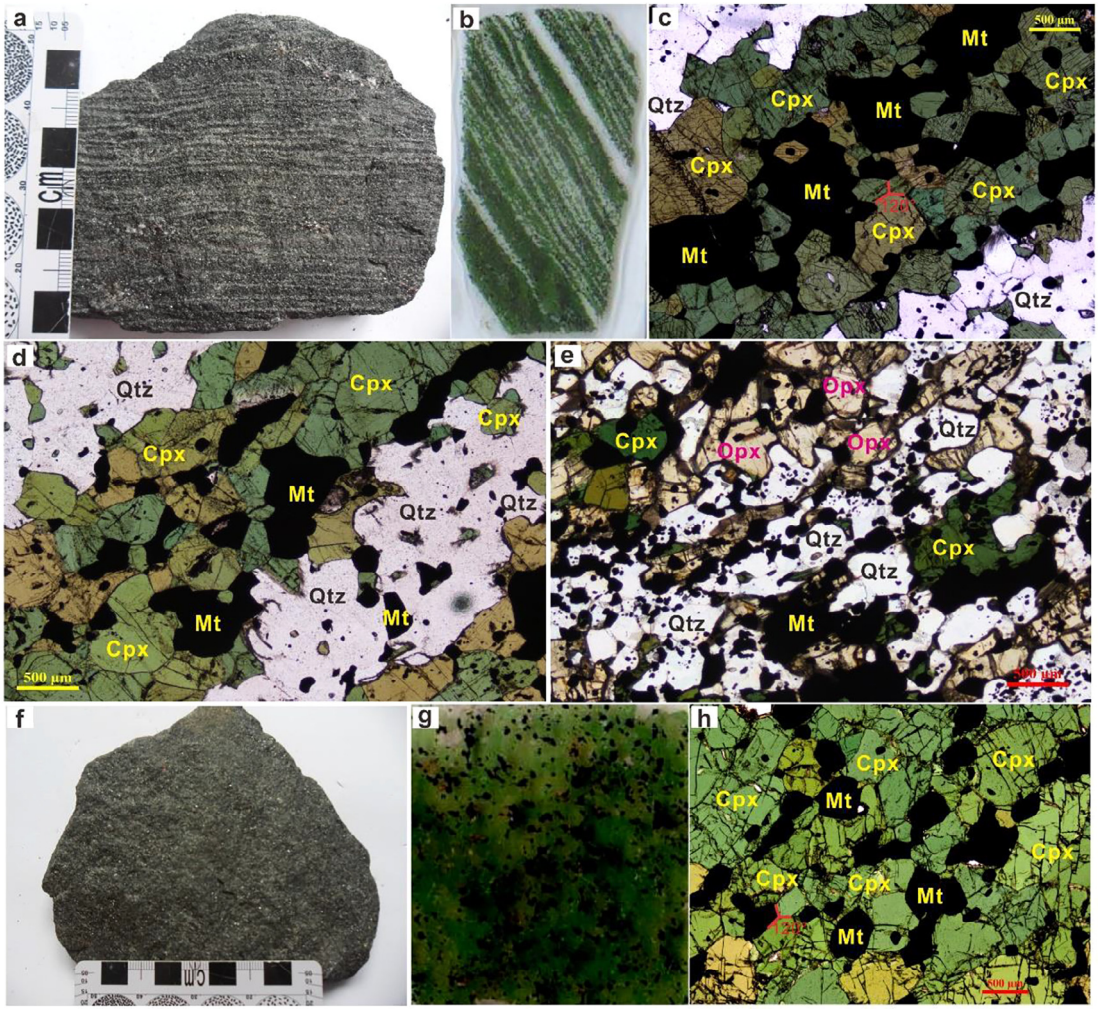


**Fig. 6.** Photomicrographs of the Wuyang BIF. (a-b) BPM in hand and section, showing clear Si-rich band and Fe-rich band. (c) Magnetite and clinopyroxene in Fe-rich band, showing grains contact in typically triple junction with 120° each other (plane-polarized light). (d) Quartz and minor magnetite in Si-rich band (plane-polarized light). (e) BPM showing clinopyroxene coexisting with orthopyroxene, quartz and magnetite (plane-polarized light). (f-g) DPM in hand and section. (h) Clinopyroxene and magnetite contact in typically triple junction with 120° each other (plane-polarized light). Qtz-quartz; Cpx-clinopyroxene; Opx-orthopyroxene; Mt-magnetite.

Banding and lamination are typical structures in the BPM samples (Fig. 6a and b). The mineral assemblages of the BPM typically consist of quartz, magnetite, and clinopyroxene (Fig. 6c and d) with subordinate orthopyroxene observed elsewhere (Fig. 6e). In most case the orthopyroxene and clinopyroxene grains occur in the same bands (Fig. 6e). The orthopyroxene in the BPM is hypersthene in content. Combined with associated clinopyroxene in the same sample, it is suggested that the Wuyang BIF has underwent granulite-facies metamorphism. The Fe-rich bands in the BPM consist of magnetite and clinopyroxene (Fig. 6c), whereas the Si-rich bands mainly comprise quartz, with minor magnetite and clinopyroxene (Fig. 6d). The clinopyroxene grains (40–45 vol %) in the Fe-rich bands are green in color and coarse-grained (0.2 to 2 mm), as well as enhedral or subhedral; they lack exsolution (Fig. 6c) and are commonly intergrown with magnetite (Fig. 6c). The quartz grains (25–30%) in the Si-rich bands are anhedral and interlocking and they are extremely variable in terms of size (0.05 to 0.5 mm). They mostly display wave extinction under optical microscopy, and they generally contain minor inclusions of dominantly magnetite (Fig. 6d). The magnetite grains in the BPM samples are mostly dispersed in the quartz or pyroxene matrix (Fig. 6c–e). The DPM samples are different from the BPM samples due to their lack of banded textures (Fig. 6f) and lower contents of quartz but higher contents of clinopyroxene (Fig. 6g and h). The magnetite grains in the DPM samples are also dispersed in the clinopyroxene matrix (Fig. 6g and h). The magnetite and pyroxene grains in DPM are commonly in contact, typically with a triple junction of 120° (Fig. 6h); this feature is similar to that observed in the BPM samples (Fig. 6c).

## 3. Analytical methods

Magnetite grains from the Xincai, Xuchang and Wuyang BIFs were selected for major and trace elemental analyses. The major element contents of magnetite crystals in polished thin sections were determined by a JEOL JXA-8230 EPMA equipped with five WDS spectrometers plus one energy-dispersive spectrometer was used to acquire backscattered electron (BSE) images and the mineral compositions of magnetite at the Key Laboratory of Mineralogy and Metallogeny, Guangzhou Institute of Geochemistry, Chinese Academy of Sciences, Guangzhou, China. The elements of interest (Si, Al, Mn, Mg, Fe, Ti, V, Ca, Ni and Cr), expressed as oxides, were analyzed using a voltage of 15 kV and a beam current of 20 nA, focused to a spot of less than 1 μm in size. Chemically analyzed natural magnetite, rhodonite, diopside, olivine, almandine garnet and rutile as well as pure vanadium and nickel served as standards. All raw data were corrected by ZAF, and V data were corrected to avoid the interference of Ti-Kβ radiation. The peak and background counting times were 20 s and 10 s for Si, Al, Fe,

Mg and Ca, 40 s and 20 s for Ti and Mn, and 60 s and 30 s for Cr, Ni and V, respectively. The EMPA data served as the basis for LA-ICP-MS data calibration.

The trace element contents of magnetite crystals in polished thin sections were determined by LA-ICP-MS at the Guangzhou Institute of Geochemistry, Chinese Academy of Sciences, Guangzhou, China. This LA-ICP-MS system consists of a Resonetics Resolution M-50 laser ablation system coupled to an Agilent 7500a Inductively Coupled Plasma Mass Spectrometer. Helium, as a carrier gas, and argon, as a makeup gas, were mixed via a T-connector prior to entering the ICP. A spot size with a diameter of 44 μm at 5 Hz was applied. Each analysis started with a 20 s measurement of the gas blank, followed by 40 s of data acquisition from the sample. Iron contents that were independently determined by EMPA were used as the internal standard to correct for the inter-element fractionation and differences during each individual analysis of magnetite. Samples were measured in short runs bracketed by the external standards Glass KL-2 and NIST SRM 610, with reference values taken from Pearce et al. (1997) and Tu et al. (2011). Detailed analytical procedures and instrumental operating conditions have been described by Tu et al. (2011). The sum of all element concentrations, expressed in oxide form (according to their oxidation states in magnetite), is considered to be 100 wt% for a given anhydrous mineral (Liu et al., 2008; Gao et al., 2013). Data processing was performed using the software ICPMSDataCal, as scripted by Liu et al. (2008). This software was also used for the integration selection of background and analysis signals, the correction of time drift and quantitative calibration. All laser ablation data were processed by non-automatic spectra reduction to exclude spectra or parts of spectra that were affected by mineral inclusions.

LA-ICP-MS trace elemental mapping was conducted at the School of Marine Sciences of the Sun Yat-sen University (Guangzhou, China), using a 193 ArF Excimer Laser Ablation system (*GeoLasPro*) coupled with an Agilent 7700X ICP-MS. The detailed equipment setting and analytical procedures and data reduction have been described by Li et al. (2018) and are briefly summarized here. A beam size of 24 μm was employed and the energy density was 5 J/cm$^2$ with a repetition rate of 10 Hz. The target area was defined by the Matrix program which consisted of rows and columns. To generate an evenly-spaced spot matrix, adjacent spots were ablated in a successive manner with no spacing in-between, and a small overlap (2 μm) was programmed to avoid unablated gaps. Finally, a square area of 600 μm × 600 μm was ablated to cover the sample (30 spots/per line × 30 lines). For data reduction, we defined a relative coordinate of the raw data to each spot by using an in-house Excel add-in and then generated the element distribution maps via the software IoGAS v6.1 (http://reflexnow.com/iogas/). It is reasonable to assume that the elemental signals along the rims of fish-debris grains are relatively low, as spot analysis ablated more matrices (e.g. resin).

## 4. Analytical results

### 4.1. LA-ICP-MS trace elemental mapping of magnetite

Representative elemental maps of magnetite from the Xuchang, Xincai and Wuyang BIFs are presented in Figs. 7–9. Inner and edge zones in magnetite grains from these BIFs are different in terms of Mg, Mn, Al, Si and Na compositions. The magnetite edge in contact with high Mg-Mn-Al hornblend and grunerite from the Xuchang and Xincai BIFs show higher Mg, Mn and Al concentrations than the inner (Figs. 7b-d and 8b-c and f). Similar features are also observed in magnetite from the Wuyang BIF. The magnetite rim closed to the high Mg-Mn-Na clinopyroxene from the Wuyang BIF also has higher Mg, Mn, Al and Na contents than the inner (Fig. 9b-c and e-f). However, these magnetite grains do not show clear Ti and V zonations (Figs. 7e-f, 8g-h and 9g-h).

### 4.2. Magnetite chemistry

#### 4.2.1. Magnetite in the Xuchang BIF

Trace element compositions of magnetite in these metamorphic BIF samples are provided in Table S1, which is available online. Trace element concentrations of magnetite in the Xuchang BIF contain high Al (243–550 ppm), variable Ti (79–411 ppm) and extremely low Mg (8–27 ppm), Mn (17–66 ppm), Zn (6–11 ppm), V (19–30 ppm), Cr (5–14 ppm), Co (less than 1 ppm), Ni (less than 3 ppm) and Ga (3–7 ppm). Compared with unmetamorphosed magnetite worldwide, these magnetite grains in the Xuchang BIFs have relatively high Al and Ti contents (Fig. 10a).

#### 4.2.2. Magnetite in the Xincai BIF

The magnetite grains in the Type I BIF have concentrations of Al (346–438 ppm), Ti (150–418 ppm), Cr (10–41 ppm) and V (21–59 ppm) higher than those of the magnetite (Al: 96–176 ppm; Ti: 29–46 ppm; Cr: 3–10 ppm; V: 6–8 ppm) grains in the Type II BIF (Table S1). In contrast, magnetite grains in the Type II BIF have Mn concentrations (up to 1146 ppm) higher than those of the Type I magnetite grains (151 to 212 ppm). Both Mg and Zn contents of magnetite from the Type II BIF are slightly higher than those from the Type I BIF. The contents of Co, Ni and Ga in the magnetite grains in both the Type I and Type II samples are extremely low and less than 5 ppm (Table S1). Compared with those published data of unmetamorphosed magnetite, Al, Ti, V and Cr contents are relatively high in these magnetite grains from the Type I samples but relatively low in magnetite from the Type II samples of the Xincai BIF (Fig. 10b).

#### 4.2.3. Magnetite in the Wuyang BIF

On the basis of their different pyroxene and magnetite compositions, the BPM samples of the Wuyang BIF can be classified as Type I and Type II. The former has clinopyroxene containing 1281 ppm Al and 90 ppm Ti, whereas the latter has clinopyroxene with much lower Al (143 ppm) and Ti (54 ppm) contents (pyroxene data are from Lan et al., under review). The magnetite grains in the Type I samples have concentrations of Mg (37–601 ppm), Zn (12–28 ppm), Al (358–849 ppm) and Ti (74–125 ppm) that are higher than those of the magnetite (Mg: 34–76 ppm; Zn: 4–18 ppm; Al: 53–99 ppm; Ti: 4–12 ppm) grains in the Type II samples (Table S1). The Mn concentrations of magnetite from both sample types are indistinguishable (385–869 ppm) (Table S1). The contents of V, Cr, Co, Ni, Ga, Ge and Sn in the magnetite grains in both the Type I and Type II samples are extremely low and less than 10 ppm (Table S1). Compared to the magnetite from the BPM samples, those in the DPM samples are characterized by variable contents of Mg (22–177 ppm), Al (131–997 ppm), Ti (77–320 ppm), Mn (436–2750 ppm) and Zn (5–40 ppm) (Table S1). The contents of other elements, such as V, Cr, Co, Ni and Ga, in the magnetite of the DPM are generally less than 10 ppm (Table S1). Compared with those published data of unmetamorphosed magnetite, Al and Ti contents are relatively higher in these magnetite grains from the Type I samples of the BPM and from the DPM samples of the Wuyang BIF (Fig. 10c and d).

## 5. Discussion

### 5.1. Initial composition of magnetite in BIF

The initial composition of magnetite in BIF is mainly controlled by the origin of magnetite and compositions of contemporary Paleo-seawater.

#### 5.1.1. The origin of magnetite in BIF

Petrographic evidence certainly implies a secondary origin for magnetite in BIFs (Ayres, 1972; Ewers and Morris, 1981). Magnetite can be the metamorphic by-product of hematite and siderite during post-diagenetic metamorphism with temperatures ranging from 480 °C

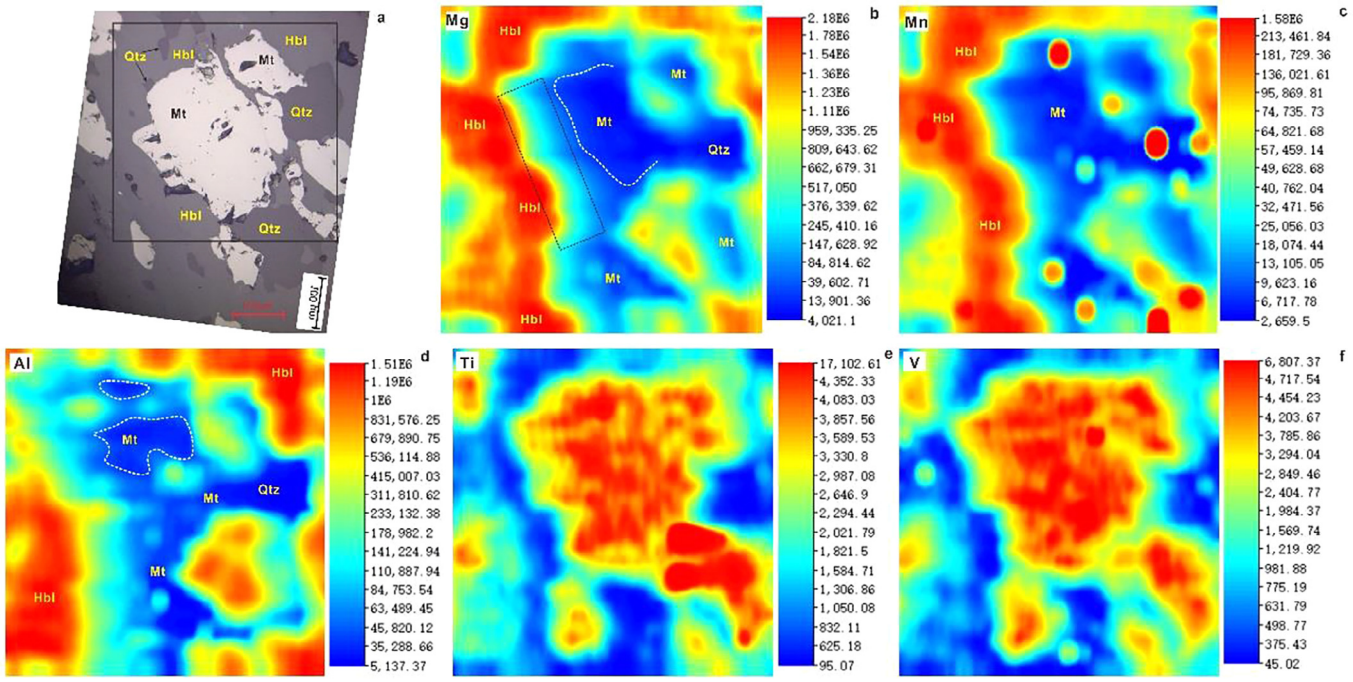


**Fig. 7.** Petrography of the ablation mapping area (a) and quantitative LA-ICP-MS trace element maps of the magnetite + hornblende + quartz assemblages from the Xuchang BIF, all maps show log ppm abundances (b-f). Qtz-quartz; Hbl-hornblende; Mt-magnetite. The box is the edge of magnetite grain in-contact with hornblende, which has elevated Mg concentration.

to 650 °C and pressures of 5–12 kbar (Ewers and Morris, 1981; Koziol, 2004), or formed through the conversion of pre-existing hematite and Fe(II)-rich hydrothermal fluids at less than 200 °C (Ohmoto, 2003; Alibert, 2016). The reduction of ferricoxyhydroxides through dissimilatory iron reduction (DIR) is also a likely source for the magnetite in BIFs at a low temperature (Lovley, 1993; Johnson et al., 2008).

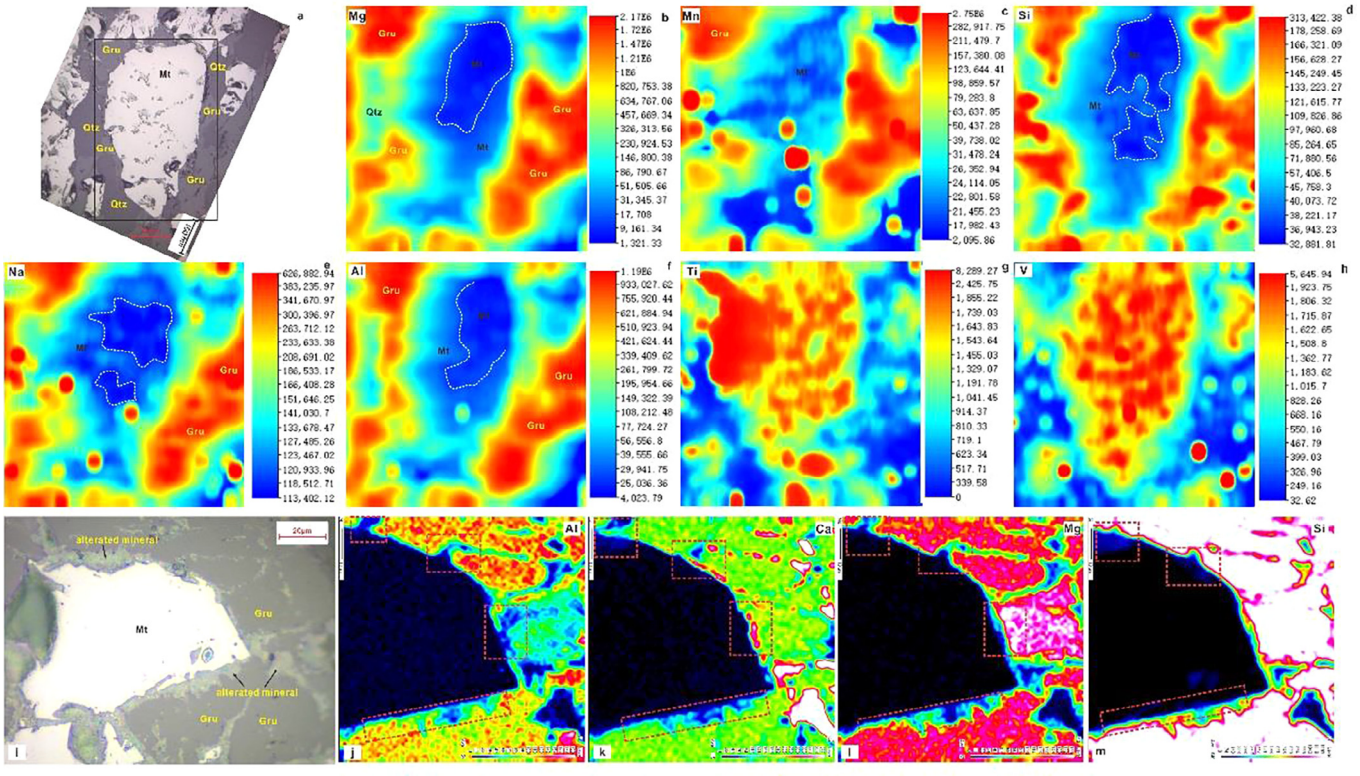


**Fig. 8.** Elemental distribution of the magnetite + grunerite + quartz assemblages from the Xincai BIF: (a) Petrography of the ablation mapping area. (b-h) Quantitative LA-ICP-MS trace element maps and all maps show log ppm abundances. The dash lines present heterogeneous composition of magnetite grains. (i) Petrography of the X-ray mapping area, showing that metamorphic fluids produced during metamorphism. (j-m) Quantitative X-ray trace element maps, showing that elements from metamorphic fluids incorporated in magnetite. Qtz-quartz; Gru-grunerite; Mt-magnetite.

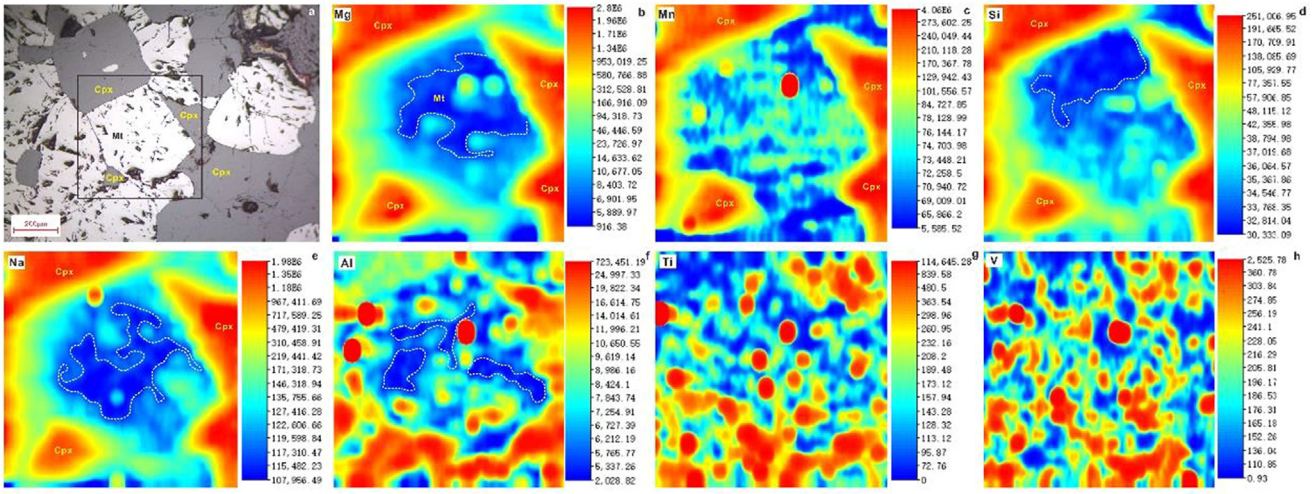


**Fig. 9.** Petrography of the ablation mapping area (a) and quantitative LA-ICP-MS trace element maps of the magnetite + clinopyroxene assemblages from the Wuyang BIF, all maps show log ppm abundances (b-h). Cpx-clinopyroxene; Mt-magnetite.

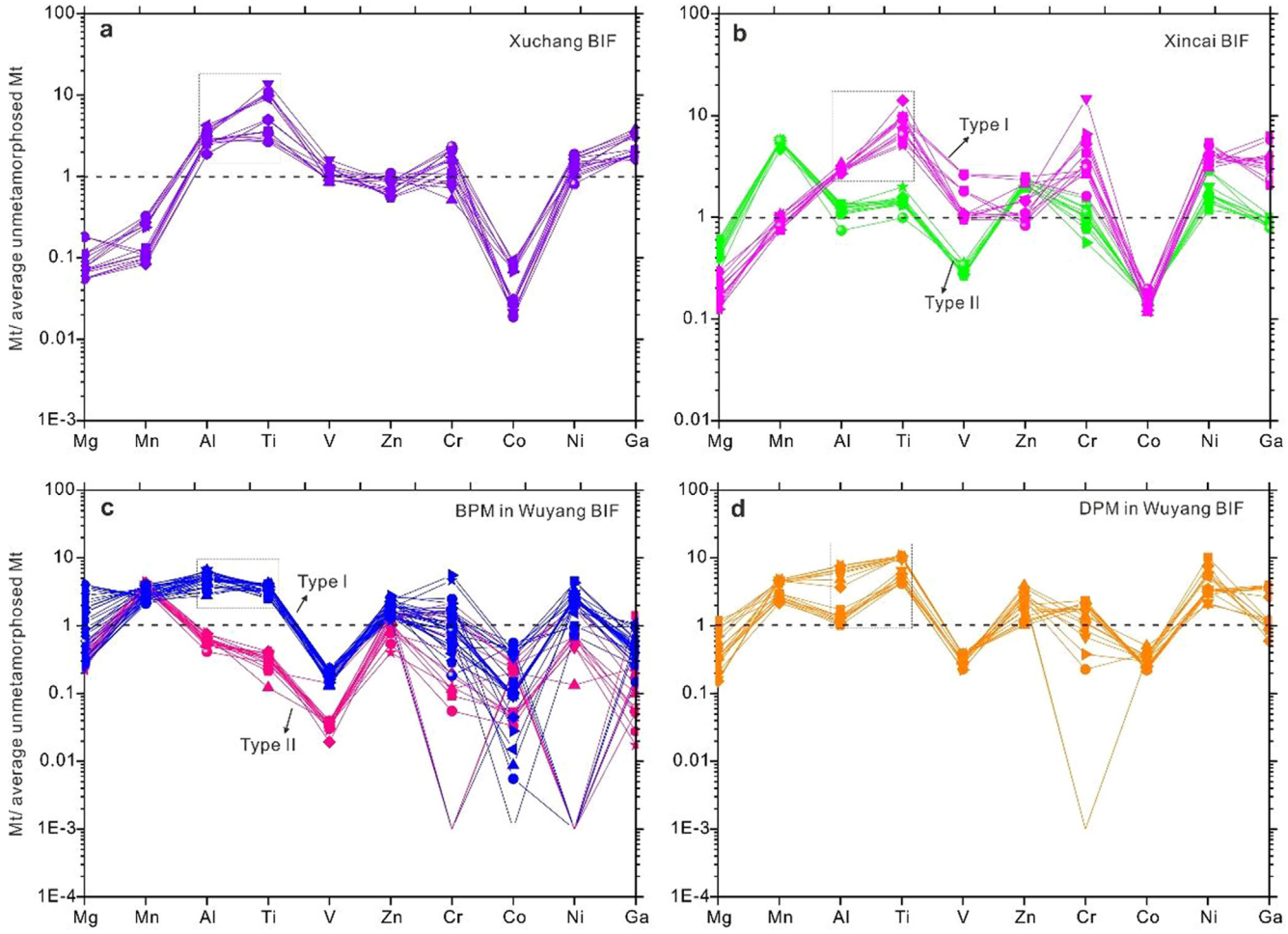


**Fig. 10.** Normalized multielemental patterns of magnetite from the Xuchang (a), Xincai (b) and Wuyang (c-d) BIFs. Normalizing values are the average composition of magnetite from the unmetamorphosed BIF from the Sokoman Iron Formation (Chung et al., 2015): Mg = 148, Mn = 201, Al = 129, Ti = 30, V = 22, Zn = 10, Cr = 6, Co = 15, Ni = 1, Ga = 2 (all in ppm). The chemical compositions of magnetite from amphibolite- to granulite-facies BIFs exhibit systematic changes of Mn, Al and Ti with increasing metamorphic temperature and can be divided into different types based on the compositions of coexsiting silicate minerals. Type I of the Xincai BIF is the magnetite coexisting with abundant biotite and grunerite, whereas Type II of the Xincai BIF is the magnetite coexisting with minor biotite and grunerite. Type I of the Wuyang BIF in Fig. 10c is magnetite coexisting with Al-Ti-rich clinopyroxene, whereas the Type II of the Wuyang BIF in Fig. 10c is magnetite coexisting with Al-Ti-poor clinopyroxene.

Recently, experiments showed that magnetite in BIF could have precipitated directly from seawater through the reaction of settling ferrihydrite and hot Fe(II)-rich hydrothermal fluids that existed in the deeper water (Li et al., 2017). Although magnetite in BIFs has different origin, oxygen isotope compositions indicated formation temperatures of the earliest hematite in BIF as low as ~25 °C, whereas the earliest magnetite in BIF between 50 °C and 100 °C and the slightly later magnetite up to ~250 °C (Konhauser et al., 2017). Klein and Fink (1976) concluded that the essentially unmetamorphosed assemblages of the Sokoman Iron Formation in the Howells River area were formed at temperature of 150 °C or less. French (1973) suggested that greenalite-containing assemblages in BIFs reflect late-diagenetic conditions with a temperature range of 100 °C to 200 °C. Some other reported that the recorded peak burial metamorphic temperatures of the BIFs from the Koolyanobbing-Marda greenstone belts and Weld Range in the Yilgarn Craton, Western Australia; the Marra Mamba and Mt Sylvia Formations in Hamersley Province, Western Australia; and the Caué Formation, Quadrilátero Ferrífero (QF), Brazil, range from 200 °C to 350 °C (Rosière and Rios, 2004; Klein, 2005; Angerer et al., 2012, 2013; Duuring and Hagemann, 2013). Obviously, magnetite always occurred in most of BIFs in a low temperature. Therefore, we consider that magnetite under a very low temperature (e.g., less than 150 °C) can represent the initial phase of itself.

#### 5.1.2. The composition of the Precambrian ocean

It is hard to directly constrains on the composition of the Precambrian oceans due to absent of modern analogues. Most studies always use the sediments (e.g., BIF) from the seawater to quantitative ascertain the seawater composition (Holland, 1984; Maliva et al., 2005). The composition of the earliest oceans was ferruginous, siliceous, possibly mildly sulfidic and contained abundance of mafic-volcanic associated trace transition elements, such as Ni, Cr, Zn (Holland, 1984; Arndt, 1991; Saito et al., 2003; Maliva et al., 2005; Konhauser et al., 2009; Mloszewska et al., 2012). Some elements in the Archean to Proterozoic seawater did not change significantly, e.g., dissolved Zn concentrations (Planavsky et al., 2010). Sulfate, Mo and Cr have an abundance in the early to middle Paleoproterozoic ocean as oxidative weathering of continent was increasing (Konhauser et al., 2011). Contemporaneous BIF can also have geochemical changes as the seawater composition changed. However, most of previous studies suggested that magnetite from Archean to Paleoproterozoic BIFs has no great differences at the same metamorphosed grade except those formed at special conditions, such as alteration by mafic rock or continental Cr flux input (Bhattacharya et al., 2007; Pecoits et al., 2009; Konhauser et al., 2011; Nadoll et al., 2014). Besides, types of BIFs (Algoma and Superior types) were formed in different geological setting (near spreading centers or island arcs and near-shore continental shelves, respectively) as continent and oceanic evolution happened (Gross, 1980). The composition of local seawater of this two different setting could be different, such as Al-Ti-rich near shore continental shelves. Mass data also suggested that no significant differences between Algoma- and Superior-type BIFs has been observed (Nadoll et al., 2014). This is possibly not hard to understand because those compatible elements (e.g., Ti, Al) have low solubility in fluids at low temperatures (Ray and Webster, 2007; Nadoll et al., 2012, 2014). Therefore, we consider that initial composition of magnetite in BIFs contain low trace elements (e.g., Mg, Al, Ti, V, Cr, Zn) although compositions of Paleo-seawater changed over time.

#### 5.1.3. Initial composition

Previous studies always considered that magnetite geochemistry in low-grade metamorphosed BIFs with metamorphic temperatures of 200 °C to 350 °C or below represent the original magnetite concentration and used them as a low temperature spectrum to compare with other types of ore deposits (Nadoll et al., 2014; Dare et al., 2014). In actually, this magnetite geochemistry has a variable range. For instance, Nadoll et al. (2014) obtained variable compositions of magnetite from the low-grade metamorphic BIFs (with metamorphic temperatures of 200 °C to 350 °C) with Mg (200 to 1000 ppm), Mn (20 to 100 ppm), Al (40 to 200 ppm), Ti (10 to 30 ppm) and other elements (V, Cr, Co, Ni, Zn) less than 10 ppm. Angerer et al. (2012) reported variable Mg (147 to 1380 ppm), Al (115 to 407 ppm) and Ti (3 to 59 ppm) contents of the low-grade metamorphic magnetite. Dare et al. (2014) reported high Al (up to 1375 ppm), Ti (~441 ppm), V (~91 ppm), Cr (~37 ppm) and Zn (~34 ppm) contents of the low-grade metamorphic magnetite. Although magnetite in those low-grade metamorphic BIFs still represent a relatively low-temperature spectrum compared with other different geological settings, e.g., porphyry ore deposit and skarn ore deposit, some elemental contents of magnetite have changed during low-grade metamorphism. Compared with above, Chung et al. (2015) reported that unmetamorphosed magnetite from the Sokoman Iron Formation has very low Mg (~148 ppm), Mn (~200 ppm), Al (~129 ppm), Ti (~30 ppm), V (~22 ppm), Zn (~10 ppm), Cr (~6 ppm), Co (15 ppm), Ni and Ga (less than 2 ppm). As BIF is marine chemical sediments, original Fe-oxides in it have lower trace elements (e.g., Mg, Mn, Al, Ti, V et al.) at such low formation temperature compared with other hydrothermal deposits. Therefore, we consider that those unmetamorphosed magnetite can represent the original composition of magnetite in BIFs, which can be used as a basic value to compare with other magnetite from different metamorphosed BIFs to further investigate the influence of metamorphism. While the low-grade metamorphic magnetite has variable chemical compositions affected by some factors which need to be further discussed in the flowing text.

### 5.2. The effects of metamorphism on modification of magnetite

#### 5.2.1. Oxygen fugacity

It should consider the effects of oxygen fugacity on magnetite geochemistry because oxygen fugacity maybe changed during metamorphism. Vanadium (e.g., +3, +4 and +5) and Cr (e.g., +2, +3 and +6) have variable valence states in nature; therefore, their incorporations in magnetite are strongly linked to oxygen fugacity (Nielsen et al., 1994; Klemme et al., 2006; Righter et al., 2006; Ryabchikov and Kogarko, 2006), because only V(III) and Cr(III) that substitute for $Fe^{3+}$, are relatively compatible with magnetite structure (Barnes and Roeder, 2001; Bordage et al., 2011; Toplis and Corgne, 2002). For example, increasing $fO_2$ could decrease the partition coefficients of V and Cr into magnetite in an iron-rich melt/liquid (Toplis and Corgne, 2002). The atomic ratio of $Fe^{2+}/Fe^{3+}$ in iron oxide can reflect oxidation state of iron (Chang et al., 2016). The oxidation state of iron is the key parameter in the magmatic oxygen fugacity calculation, and the $Fe^{3+}/\Sigma Fe$ ratio of magma can be used to estimate their oxygen fugacity (Bézos and Humler, 2005). Based on this, we considered that atomic ratio of $Fe^{2+}/Fe^{3+}$ in magnetite can coarsely estimate the oxygen fugacity change. It can conclude that weak changes in oxygen fugacity occur during metamorphism based on very narrow range of $Fe^{2+}/Fe^{3+}$ ratios of the amphibolite-facies metamorphosed magnetite (from 0.4896 to 0.5056; ave. 0.5021) and of the granulite-facies metamorphosed magnetite (from 0.4940 to 0.5073; ave. 0.5017) (Table S1). The Cr and V contents in these variably metamorphosed magnetite grains are variable, but not over a wide range (less than 30 ppm), and lack of a strong positive correlation between them (Fig. 11). Therefore, the effect of oxygen fugacity on the modification of magnetite chemistry may be negligible during metamorphism.

#### 5.2.2. Metamorphic temperature

Metamorphic temperatures from the low- to high-grade metamorphosed BIFs are highly variable: approximately 200 °C to 350 °C for the greenschist-facies metamorphosed BIF, 350 °C to 640 °C for the amphibolite-facies metamorphosed BIF and ≥750 °C for the granulite-facies metamorphosed BIF. Magnetite grains from the amphibolite- to granulite-facies BIFs display low Cr, Co, Ni and Ga contents (less than

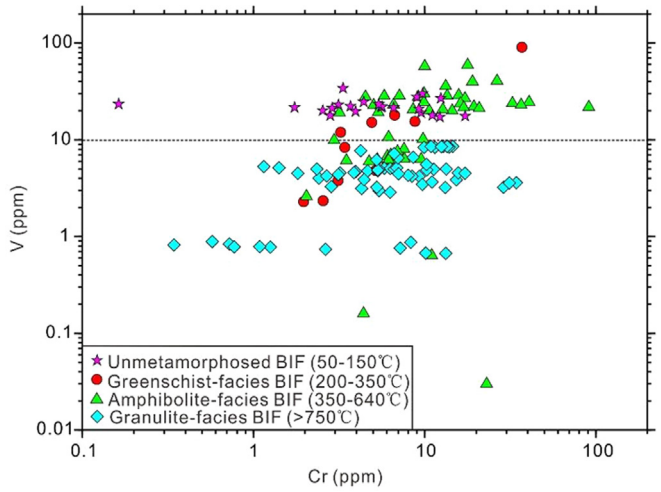


**Fig. 11.** Chromium vs. V diagram of magnetite from the unmetamorphosed and variously metamorphosed BIFs (values in ppm). Data from selected magnetite from unmetamorphosed BIF (Chung et al., 2015), greenschist-facies BIFs (Angerer et al., 2012; Dare et al., 2014; Nadoll et al., 2014), amphibolite-facies BIFs (Dai, 2014 and this paper) and granulite-facies BIF in the Wuyang area (this paper). There is no obviously strong positive correlation between the Cr and V contents in magnetite from unmetamorphosed BIF to variously metamorphosed BIFs.

10 ppm) and slightly variable V and Zn contents, and their contents do not show clear correlations with metamorphic temperatures, indicating that these elements are immobile as temperature changed. Aluminum and Ti incorporation in magnetite is largely temperature-controlled in igneous systems, and tend to enriched in magnetite forming in relatively high temperatures (Nielsen et al., 1994; Toplis and Carroll, 1995). Temperatures recorded for hydrothermal alteration and vein formation generally lie below magmatic temperatures. Nadoll et al. (2014) found that Al and Ti have on average considerably greatly concentrations in igneous magnetite than for hydrothermal occurrences on a deposit scale and considered that temperature is a major governing factor for the composition of hydrothermal magnetite. Compared with those published data of unmetamorphosed magnetite, the magnetite in relatively high-temperature, amphibolite- to granulite-facies metamorphosed BIFs have elevated Mn, Al and Ti (Fig. 10), indicative of effects of metamorphic temperatures. Besides, the diagrams of Ti/V ratio vs. Al and Ti vs. V also display clear rising trends of Al and Ti as temperature (Fig. 12). Besides, elements which occupied the same site in magnetite crystal have a negative relationship with each other in composition. High Mn contents in the amphibolite- to granulite-facies metamorphosed magnetite thus lead to low Mg contents in them (Fig. 10).

### 5.2.3. Coexisting mineral

The gangue minerals in BIFs react with each other under special conditions during metamorphism, leading to the formation of new Fe-rich silicates (e.g., amphiboles, pyroxenes, and fayalite) and fluids by the following dehydration or decarbonation reactions (Klein, 2005), followed by the reactions below:

$$\underset{\text{greenalite}}{Fe_6Si_4O_{10}(OH)_8} + 4SiO_2 \rightarrow \underset{\text{minnesotaite}}{2Fe_3Si_4O_{10}(OH)_2} + 2H_2O \quad (1)$$

$$\underset{\text{greenalite}}{Fe_6Si_4O_{10}(OH)_8} + O_2 \rightarrow \underset{\text{minnesotaite}}{2Fe_3Si_4O_{10}(OH)_2} + \underset{\text{magnetite}}{2Fe_3O_4} + 3H_2O \quad (2)$$

$$\underset{\text{siderite}}{FeCO_3} + 4SiO_2 + H_2O \rightarrow \underset{\text{minnesotaite}}{Fe_3Si_4O_{10}(OH)_2} + 2CO_2 \quad (3)$$

$$\underset{\text{stilpnomelane-like}}{Fe_{2.7}(Si, Al)_4(O, OH)_{12}\cdot\chi H_2O} + 0.33Fe^{2+} \rightarrow \underset{\text{minnesotaite}}{Fe_3Si_4O_{10}(OH)_2} + 2H_2O + Al + \text{minor(Na, K)} \quad (4)$$

$$\underset{\text{ferrodolomite}}{7Ca(Fe, Mg)(CO_3)_2} + 8SiO_2 + H_2O \rightarrow \underset{\text{grunerite}}{(Fe, Mg)_7Si_8O_{22}(OH)_2} + \underset{\text{calcite}}{7CaCO_3} + 7CO_2 \quad (5)$$

$$\underset{\text{siderite}}{8(Fe, Mg)CO_3} + 8SiO_2 + H_2O \rightarrow \underset{\text{grunerite}}{(Fe, Mg)_7Si_8O_{22}(OH)_2} + 7CO_2 \quad (6)$$

$$\underset{\text{minnesotaite}}{7Fe_3Si_4O_{10}(OH)_2} \rightarrow \underset{\text{grunerite}}{3Fe_7Si_8O_{22}(OH)_2} + 4SiO_2 + 4H_2O \quad (7)$$

$$\underset{\text{ankerite}}{Ca(Fe, Mg)(CO_3)_2} + 2SiO_2 \rightarrow \underset{\text{clinopyroxene}}{Ca(Fe, Mg)Si_2O_6} + 2CO_2 \quad (8)$$

$$\underset{\text{siderite}}{(Fe, Mg)CO_3} + SiO_2 \rightarrow \underset{\text{orthopyroxene}}{(Fe, Mg)SiO_3} + CO_2 \quad (9)$$

$$\underset{\text{grunerite}}{Fe_7Si_8O_{22}(OH)_2} \rightarrow \underset{\text{orthopyroxene}}{7FeSiO_3} + SiO_2 + H_2O \quad (10)$$

These metamorphic reactions in BIFs are essentially isochemical except for prevalent dehydration and decarbonation. Theoretically, no metamorphic reactions happened between magnetite and these gangue

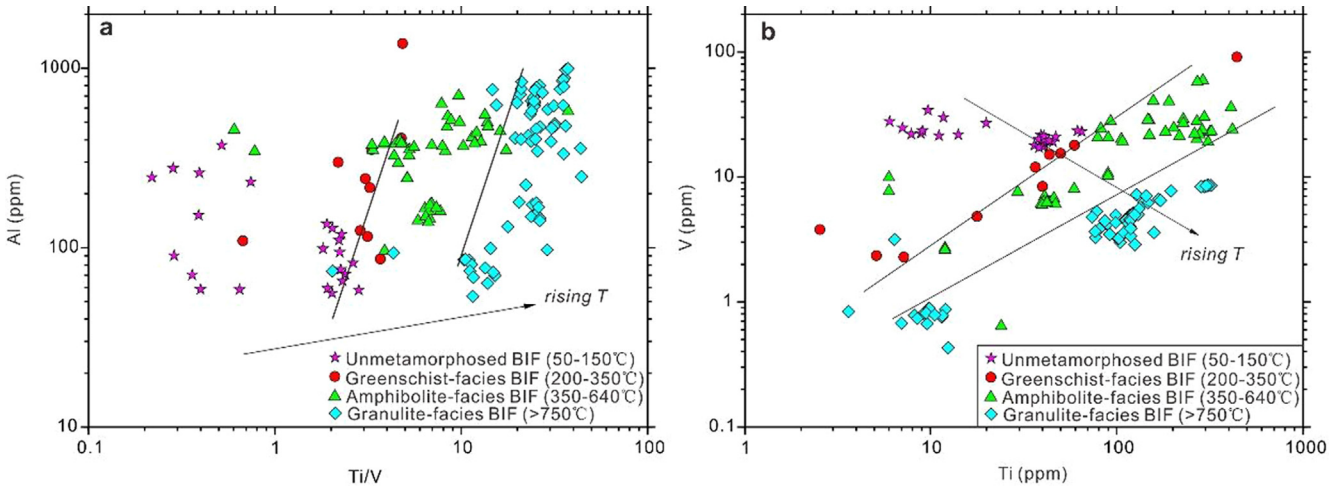


**Fig. 12.** (a) Ti/V ratio vs. Al diagram of magnetite from different metamorphosed grade BIFs with different metamorphic temperature. (b) Titanium vs. V diagram for the different metamorphic grade magnetite (values in ppm). A rising Al and Ti/V ratio, and a decreasing V and rising Ti as temperature increases can be observed in different metamorphosed grade magnetite, compared to unmetamorphosed magnetite, respectively. Data from selected magnetite from unmetamorphosed BIF (Chung et al., 2015), greenschist-facies BIFs (Angerer et al., 2012; Dare et al., 2014; Nadoll et al., 2014), amphibolite-facies BIFs (Dai, 2014 and this paper) and granulite-facies BIF in the Wuyang area (this paper).

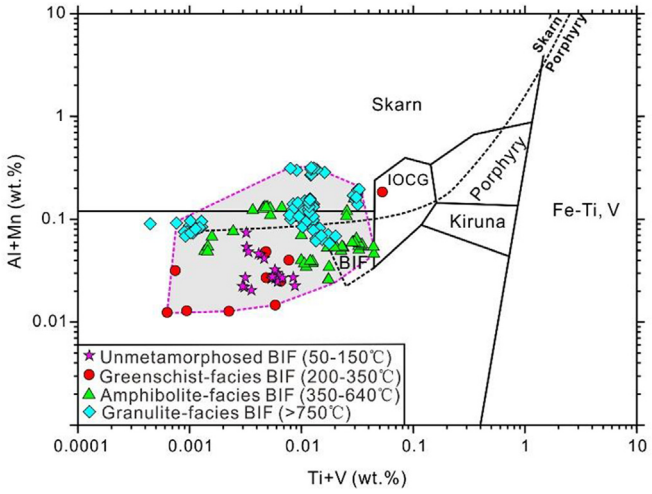


**Fig. 13.** Magnetite discrimination plots for various ore deposit types by Nadoll et al. (2014) (Al + Mn vs. Ti + V (wt.%)) using data from selected magnetite from unmetamorphosed BIF (Chung et al., 2015), greenschist-facies BIFs (Angerer et al., 2012; Dare et al., 2014; Nadoll et al., 2014), amphibolite-facies BIFs (Dai, 2014 and this paper) and granulite-facies BIF in the Wuyang area (this paper).

minerals or new-formed Fe-silicates. However, mass data show that the trace elemental variations of magnetite are correlated with the coexisting minerals of different metamorphic grades. For instance, magnetite from the greenschist-facies metamorphosed BIFs with Al-rich gangue minerals (e.g., feldspar, biotite) has extremely high concentrations of Al (up to 1375 ppm Al) and Ti (Table S1). The Al, Ti and V contents in magnetite from the amphibolite-facies metamorphosed BIFs containing minor grunerite and biotite (Type II) are lower than those in BIFs containing abundant grunerite and biotite (Type I) (Fig. 10b). In the granulite-facies metamorphosed BIFs, magnetite associated with low-Al-Ti clinopyroxene (Type II) has lower contents of Al, Ti and V than those associated with high-Al-Ti clinopyroxene (Type I) (Fig. 10c). Trace elemental mapping suggests further that the edge of magnetite grains in contact with these Fe-silicates (hornblende, grunerite, pyroxene) shows zones of elevated Mg, Mn, Al, Si, Na and their inner is depleted in these elements (Figs. 7–9), indicating that elemental diffusion and exchange between magnetite and these Fe-silicates greatly happened in high-grade metamorphism. Mueller (1967) also concluded that elemental diffusion and exchange can be used to interpret compositional changes of adjacent minerals as an important mechanism during isochemical process.

#### 5.2.4. Metamorphic fluids

Element activity is very extensive and strong in hydrothermal fluids, which is the most important control factors for minor and trace element concentrations in hydrothermal magnetite (Nadoll et al., 2014). For instance, fluids associated with skarn deposits always are enriched in K, Ca, Mn, Zn et al (Meinert et al., 2005). Above provided metamorphosed reactions in BIFs can produce some fluids at different metamorphosed temperature. These fluids either contained alkaline elements (e.g., K, Na; e.g., reaction (4)) or produced by (K, Na)-bearing silicates (e.g., grunerite) may scrape elements (e.g., Al) from these Fe-silicates. It is observed that the metamorphic fluids occurred in the amphibolite-facies Xincai BIF and Si, Ca and Al from the fluids cutting in-contact silicates incorporated into magnetite (Fig. 8i–m), although fluids from those metamorphic reactions are not very (K, Na)-rich and maybe have no greatly effects on elemental changes of the system compared with classical hydrothermal ore deposits (e.g., skarn). Alternatively, our previous work considered that pyroxene in the Wuyang BIF is not a product of reaction between pre-existing minerals but dehydration and recrystallization of original Ca-Fe-Mg-Mn gel. And dehydration was happened at diagenetic stage and it was dry during metamorphism in later-stage (Lan et al., under review). In this case, no metamorphic fluid was produced. Elemental diffusion and exchange happened by other way, such as pressure solution, except metamorphic fluids during metamorphism.

### 5.3. Implications for provenance discrimination

Most of trace elements (e.g., Mg, Mn, Al, Ti) in magnetite from BIFs are more or less changed, while the other elements (e.g., Zn, V, Cr, Co, Ni, Ga) in magnetite from various metamorphosed BIFs have no clear changes during metamorphism based on above discussion. The latter can be used to genetic discrimination of magnetite although their contents are low. The reduction of Mg and increase in Al, Ti and Mn contents in magnetite from metamorphosed BIFs suggested that elemental diffusion and exchange happened between coexisting silicate minerals and magnetite. The elements of Mg, Mn, Al and Ti in magnetite from metamorphosed BIFs are greatly controlled by metamorphic temperature and coexisting minerals. Aluminum and Ti in magnetite from metamorphosed BIFs are especially affected by coexisting silicate minerals because magnetite grains in BIFs with mass of silicate minerals or Al-Ti-rich pyroxenes have higher Al and Ti contents than those in BIFs with minor silicates minerals or Al-Ti-poor pyroxenes under the same metamorphosed temperature, respectively (Fig. 10b and c).

Previous studies have used a statistical approach, e.g., principal component analysis (Grigsby, 1990; Nadoll et al., 2012) or empirical approaches based on large databases of magnetite composition to identify combinations of elements and/or element ratios which is the most diagnostic for discrimination purposes (Dupuis and Beaudoin 2011; Nadoll et al., 2014). Data of these magnetite compositions were from different magmatic and hydrothermal setting with special magnetite composition (Reguir et al., 2008; Pecoits et al., 2009; Rusk et al., 2010; Dare et al., 2012; Angerer et al., 2013). The elements of Ti, Al, V, Ni, Cr, Mn and Ca have been used to discriminate between different types of iron ores such as BIF, skarn, porphyry and Kiruna ores (Dupuis and Beaudoin, 2011; Nadoll et al., 2014). As Ni and Cr concentrations in magnetite from BIF are very low and have no greatly changes during metamorphism, we focus on the Ti, Al, V and Mn diagram by Nadoll et al. (2014). We put all the data including from the unmetamorphosed to high-grade metamorphic BIFs on the diagram and found that the values of Ti + V and Al + Mn of these metamorphic magnetite grains were still different from any other types of hydrothermal and magmatic ore deposits except overlap with skarn deposit (Fig. 13). The overlap area is mainly the high-grade metamorphosed magnetite and our study reveals that some elements (Al and Ti) in magnetite can up to 10 times compared to those unmetamorphosed magnetite during high temperature (Fig. 10c and d). Therefore, it should be caution when we used high-grade metamorphosed (especially granulite-facies metamorphosed) magnetite chemistry to discriminate ore type. We found great temperature and coexisting mineral dependence of Al and Ti in magnetite, which can be used as an importantly considerable factor to other hydrothermal ore deposits.

## 6. Conclusions

1) Magnetite grains from the amphibolite- to granulite-facies BIFs display low Cr, Co, Ni and Ga contents and slightly variable V and Zn contents. These elemental concentrations have no great changes in magnetite during high temperature metamorphism.
2) Compared with those published data of unmetamorphosed magnetite, a rising trend of Al, Ti and Mn concentrations in the amphibolite- to granulite-facies metamorphosed magnetite as temperature increase, indicative of greatly temperature dependence.
3) Elemental diffusion and exchange between magnetite and coexisting silicate minerals are relatively extensive under high-grade metamorphism by metamorphic fluids or other way, such as pressure

solution.

4) Our study reveals that some elements (Al and Ti) in magnetite can up to 10 times compared to those in unmetamorphosed BIF during high temperature. Therefore, it should be caution when we used high-grade metamorphosed (especially granulite-facies metamorphosed) magnetite chemistry to discriminate ore type.

## Acknowledgments

We appreciate the field assistance of geologists from the Wuyang Mine, especially Yuanyou Zhang and Huaiqian Li. Changming Xing and Congyin Li are greatly acknowledged for their lab support. We are grateful to the careful and constructive comments of Prof. Zhaochong Zhang and two anonymous reviewers. This study was supported by the National Natural Science Foundation of China (Nos. 41602078 and 41573041).

## Appendix A. Supplementary data

Supplementary data to this article can be found online at https://doi.org/10.1016/j.oregeorev.2019.103019.

## References

Ahmad, S.N., Rose, A.W., 1980. Fluid inclusions in porphyry and skarn ore at Santa Rita, New Mexico. Econ. Geol. 75, 229–250.
Alibert, C., 2016. Rare earth elements in Hamersley BIF minerals. Geochim. Cosmochim. Acta 184, 311–328.
Angerer, T., Hagemann, S.G., Danyushevsky, L.V., 2012. Geochemical evolution of the banded iron formation-hosted high-grade iron ore system in the Koolyanobbing greenstone belt, Western Australia. Econ. Geol. 107 (4), 599–644.
Angerer, T., Hagemann, S.G., Danyushevsky, L., 2013. High-grade iron ore at Windarling, Yilgarn Craton: a product of syn-orogenic deformation, hypogene hydrothermal alteration and supergene modification in an Archean BIF-basalt lithostratigraphy. Miner. Deposita 48, 697–728.
Arndt, N.T., 1991. High Ni in Archean tholeiites. Tectonophysics 187, 411–419.
Ayres, D.E., 1972. Genesis of iron-bearing minerals in banded iron formation mesobands in The Dales Gorge Member, Hamersley Group, Western Australia. Econ. Geol. 67, 1214–1233.
Barnes, S.J., Roeder, P.L., 2001. The range of spinel compositions in terrestrial mafic and ultramafic rocks. J. Petrol. 42 (12), 2279–2302.
Bekker, A., Slack, J.F., Planavsky, N., Krapež, B., Hofmann, A., Konhauser, K.O., Rouxel, O.J., 2010. Iron formation: the sedimentary product of a complex interplay among mantle, tectonic, oceanic, and biospheric processes. Econ. Geol. 105, 467–508.
Bézos, A., Humler, E., 2005. The $Fe^{3+}/\Sigma Fe$ ratios of MORB glasses and their implications for mantle melting. Geochim. Cosmochim. Acta 69, 711–725.
Bhattacharya, H.N., Chakrabortym, I., Ghosh, K.K., 2007. Geochemistry of some banded iron-formations of the Archean Supracrustals, Jharkhand-Orissa region, India. J. Earth Syst. Sci. 116, 245–259.
Bonnichsen, B., 1969. Metamorphic pyroxenes and amphiboles in the Biwabik Iron Formation, Dunka River area, Minnesota. Mineralogical Society of America Special Paper 2, 217–241.
Bordage, A., Balan, E., De Villiers, J.P.R., Cromarty, R., Juhin, A., Carvallo, C., Calas, G., Raju, P.V.S., Glatzel, P., 2011. V oxidation state in Fe-Ti oxides by high-energy resolution fluorescence-detected X-ray absorption spectroscopy. Phys. Chem. Miner. 38 (6), 449–458.
Bragg, W.H., 1915. The structure of the spinel group of crystals. Phil. Mag. 30, 305–315.
Buddington, A.F., Lindsley, D.H., 1964. Iron-titanium oxide minerals and synthetic equivalents. J. Petrol. 5, 310–357.
Chang, Y.H., Ou, C.C., Yeh, H.W., Yang, C.S., 2016. Photo-catatytic selectivity of anthranilic acid over iron oxide incorporated titanic nanoparticles: influence of the $Fe^{2+}/Fe^{3+}$ ratio of iron oxide. J. Mol. Catal. A: Chem. 412, 67–77.
Chen, W.T., Zhou, M.F., Gao, J.F., Hu, R.Z., 2015. Geochemistry of magnetite from Proterozoic Fe-Gu deposit in the Kangdian mtallogenic province, SW China. Miner. Deposita 50, 795–809.
Chung, D., Zhou, M.F., Gao, J.F., Chen, W.T., 2015. In-situ LA-ICP-MS traceelemental analyses of magnetite: the late PalaeoproterozoicSokoman Iron Formation in the Labrador Trough, Canada. Ore Geol. Rev. 65, 917–928.
Cui, L.Y., Wang, F.S., Wang, J.Z., 2008. Investigation Report on Iron Ore in the Xincai Area Henan Province. Geology Investigation Institute of Henan Province, pp. 1–105 (in Chinese).
Dai, Y.P., 2014. The Archean Two-stage BIF Deposition and Genesis of High-Grade Iron Ores in the Anshan-Benxi Area. Ph.D. thesis. the Graduate School of the Chinese Academy of Sciences, Beijing.
Dare, S.A.S., Barnes, S.J., Beaudoin, G., 2012. Variation in trace element content of magnetite crystallized from a fractionating sulfide liquid, Sudbury, Canada: implications for provenance discrimination. Geochim. Cosmochim. Acta 88, 27–50.
Dare, S.A.S., Barnes, S.J., Beaudoin, G., Méric, J., Boutroy, E., Potvin-Doucet, C., 2014. Trace elements in magnetite as petrogenetic indicators. Miner. Deposita 49, 785–796.
Diwu, C.R., Sun, Y., Guo, A.L., Wang, H.L., Liu, X.M., 2011. Crustal growth in the North China Craton at ~2.5 Ga: evidence from in situ zircon U-Pb ages, Hf isotopes and whole-rock geochemistry of the Dengfeng complex. Gondwana Res. 20, 149–170.
Diwu, C.R., Sun, Y., Zhao, Y., Lai, S., 2014. Early Paleoproterozoic (2.45-2.20 Ga) magmatic activity during the period of global magmatic shutdown: implications for the crustal evolution of the southern North China Craton. Precambr. Res. 255, 627–640.
Dupuis, C., Beaudoin, G., 2011. Discriminant diagrams for iron oxide trace element fingerprinting of mineral deposit types. Miner. Deposita 46, 319–335.
Duuring, P., Hagemann, S., 2013. Leaching of silica bands and concentration of magnetite in Archean BIF by hypogene fluids: Beebyn Fe ore deposit, Yilgarn Craton, Western Australia. Miner. Deposita 48, 341–370.
Evans, B.W., Frost, B.R., 1975. Chrome-spinel in progressive metamorphism-preliminary analysis. Geochim. Cosmochim. Acta 39, 959–972.
Ewers, W., Morris, R., 1981. Studies of the Dales Gorge Member of the Brockman Iron Formation, Western Australia. Econ. Geol. 76, 1929–1953.
Fleet, M.E., 1981. The structure of magnetite. Acta Crystallogr. Section B-Struct. Sci. 37, 917–920.
French, B.M., 1968. Progressive contact metamorphism of the Biwabik Iron Formation, Mesabi Range, Minnesota. Minnesota Geol. Survey Bull. 45, 1–103.
French, B.M., 1973. Mineral assemblages in diagenetic and low-grade metamorphic iron formation. Econ. Geol. 68, 1063–1074.
Frost, B.R., 1991. Stability of oxide minerals in metamorphic rocks. In: Lindsley, D.H. (Ed.), Oxide Minerals: Petrologic and Magnetic Significance. Reviews in Minerology. Mineralogical Society of America, pp. 467–487.
Frost, B.R., Lindsley, D.H., 1991. Occurrence of iron-titanium oxides in igneous rocks. In: Lindsley, D.H. (Ed.), Petrologic and Magnetic Significance. Reviews in Minerology. Mineralogical Society of America, pp. 433–468.
Gao, J.F., Zhou, M.F., Lightfoot, P.C., Wang, C.Y., Qi, L., Sun, M., 2013. Sulfide saturation and magma emplacement in the formation of the Permian Huangshandong Ni-Cu sulfide deposit, Xinjiang, northwestern China. Econ. Geol. 108 (8), 1833–1848.
GIIHP, 2008. In: Report of Iron deposit in the Wuyang-Xincai Areas. Henan Province by Geology Investigation Institute of Henan Province, pp. 1–120 in Chinese.
Grigsby, J.D., 1990. Detrital magnetite as a provenance indicator. J. Sediment. Petrol. 60 (6), 940–951.
Gross, G.A., 1980. A classification of iron-formation based on depositional environments. Can. Mineral. 18, 215–222.
HBGMR, 1989. In: Regional Geology of Henan Province. Geological Publishing House, Beijing, pp. 1–772 in Chinese.
Holland, H.D., 1984. The Chemical Evolution of the Atmosphere and Oceans. Princeton University Press, Princeton, NJ.
Huang, H., Zhang, L.C., Sébastien, F., Wang, C.L., Zhai, M.G., 2016. Depositional environment and origin of the Lilaozhuang Neoarchean BIF-hosted iron–magnesite deposit on the southern margin of the North China Craton. Int. J. Earth Sci. 106 (5), 1753–1772.
Huang, H., 2014. The minralizing age, forming evvironment and genesis of Huoqiu BIF ironstone in southern margin of the North China Craton, Ph.D. thesis, the Graduate School of the Chinese Academyof Sciences, Beijing, 27–79 (in Chinese with English abstract).
Isley, A.E., 1995. Hydrothermal plumes and the delivery of iron to banded iron formation. J. Geol. 103, 169–185.
Jahn, B.M., Ernst, W.G., 1990. Late Archean Sm-Nd Isochron Age for Mafic-Ultramafic Supracrustal Amphibolites from the Northeastern Sino-Korean Craton, China. Precambr. Res. 46 (4), 295–306.
James, H.L., 1954. Sedimentary facies of iron-formation. Econ. Geol. 49, 235–293.
Johnson, C.M., Beard, B.L., Klein, C., Beukes, N.J., Roden, E.E., 2008. Iron isotopes constrain biologic and abiologic processes in banded iron formation genesis. Geochim. Cosmochim. Acta 72, 151–169.
Klein, C., 1978. Regional metamorphism of Proterozoic iron-formation, Labrador Trough, Canada. Am. Mineral. 63, 898–912.
Klein, C., 2005. Some Precambrian banded iron-formations (BIFs) from around the world: their age, geologic setting, mineralogy, metamorphism, geochemistry, and origins. Am. Mineral. 90, 1473–1499.
Klein, C., Fink, R.P., 1976. Petrology of the Sokoman Iron Formation in the Howells River area, at the western edge of the Labrador Trough. Econ. Geol. 71, 453–487.
Klemme, S., Günther, D., Hametner, K., Prowatke, S., Zack, T., 2006. The partitioning of trace elements between ilmenite, ulvospinel, annalcolite and silicate melts with implications for the early differentiation of the moon. Chem. Geol. 234, 251–263.
Konhauser, K.O., Pecoits, E., Lalonde, S.V., Papineau, D., Nisbet, E.G., Barley, M.E., Arndt, N.T., Zahnle, K., Kamber, B.S., 2009. Oceanic nickel depletion and a methanogen famine before the Great Oxidation Event. Nature 458, 750–753.
Konhauser, K.O., Lalonde, S.V., Planavsky, N.J., Pecoits, E., Lyons, T.W., Mojzsis, S.J., Rouxel, O.J., Barley, M.E., Rosiere, C., Fralick, P.W., Kump, L.R., Bekker, A., 2011. Aerobic bacterial pyrite oxidation and acid rock drainage during the Great Oxidation Event. Nature 478 (7369), 369–373.
Konhauser, K.O., Planavsky, N.J., Hardisty, D.S., Robbins, L.J., Warchola, T.J., Haugaard, R., Lalonde, S.V., Partin, C.A., Oonk, P.B.H., Tsikos, H., Lyons, T.W., Bekker, A., Johnson, C.M., 2017. Iron formations: a global record of Neoarchaean to Palaeoproterozoic environmental history. Earth Sci. Rev. 172, 140–177.
Koziol, A.M., 2004. Experimental determination of siderite stability and application to Martian Meteorite ALH84001. Am. Mineral. 89, 294–300.
Kröner, A., Compston, W., Zhang, G.W., Guo, A.L., Todt, W., 1988. Age and tectonicsetting of Late Archean greenstone-gneiss terrain in Henan Province, China, asrevealed by single-grain zircon dating. Geology 16, 211–215.
Kusky, T.M., Li, J.H., Tucker, R.D., 2001. The Archean Dongwanzi ophiolite complex, North China craton: 2.505-billion-year-old oceanic crust and mantle. Science 292

(5519), 1142–1145.
Lan, C.Y., 2015. Origin of the Early Precambrian Wuyang Iron Deposit in the Southern Margin of the North China Craton. Ph.D. thesis. the Graduate School of the Chinese Academy of Sciences, Beijing, pp. 1–104.
Lan, C.Y., Long, X.P., Zhao, T.P., Zhai, M.G. In-site mineral geochemistry and whole-rock Fe isotopes of the quartz-magnetite-pyroxene rocks in the Wuyang area, North China Craton: Constraints on the genesis of the pyroxene-rich BIF. Submit to Precambrian Research, under review.
Lan, C.Y., Zhou, Y.Y., Wang, C.L., Zhao, T.P., 2017. Depositional age and protoliths of the Paleoproterozoic upper Taihua Group in the Wuyang area in the southern margin of the North China Craton: new insights into stratigraphic subdivision and tectonic setting. Precambr. Res. 297, 77–100.
Lan, C.Y., Yang, A.Y., Wang, C.L., Zhao, T.P., 2019. Geochemistry, U-Pb zircon geochronology and Sm-Nd isotopes of the Xincai banded iron formation in the southern margin of the North China Craton: implications on Neoarchean seawater compositions and solute sources. Precambr. Res. 326, 240–257.
Li, D.F., Fu, Y., Sun, X.M., Hollings, P., Liao, J.L., Liu, Q.F., Feng, Y.Z., Liu, Y., Lai, C., 2018. LA-ICP-MS trace element mapping: Element mobility of hydrothermal magnetite from the giant Beiya Fe-Au skarn deposit, SW China. Ore Geol. Rev. 92, 463–474.
Li, Y.L., Konhauser, K.O., Zhai, M.G., 2017. The formation of magnetite in the early Archean oceans. Earth Planet. Sci. Lett. 466, 103–114.
Liang, Y.H., Yu, S.J., Li, S.Z., Yang, J.L., 1981. The study of the Late Archaeozoic strata and iron-bearing horizons in the central Henan and western Anhui. J. Yichang Inst. Geol. Mineral Resour., Chinese Acad. Geol. Sci. 3, 21–39 (in Chinese with English abstract).
Lindsley, D.H., 1976. The crystal chemistry and structure of oxide minerals as exemplified by the Fe-Ti oxides. In: Rumble, D. (Ed.), Oxide Minerals. Reviews in Minerology. Mineralogical Society of America, pp. 1–60.
Liu, Y.S., Hu, Z.C., Gao, S., Günther, D., Xu, J., Gao, C.G., Chen, H.H., 2008. In situ analysis of major and trace elements of anhydrous minerals by LA-ICP-MS without applying an internal standard. Chem. Geol. 257, 34–43.
Liu, D.Y., Nutman, A.P., Compston, W., Wu, J.S., Shen, Q.H., 1992. Remnants of 3800 Ma crust in the Chinese part of the Sino-Korean Craton. Geology 20, 339–342.
Liu, L., Yang, X.Y., 2015. Temporal, environmental and tectonic significance of the Huoqiu BIF, southeastern North China Craton: geochemical and geochronological constraints. Precambr. Res. 261, 217–233.
Lovley, D.R., 1993. Dissimilatory metal reduction. Annu. Rev. Microbiol. 47, 263–290.
Lu, J.S., Wang, G.D., Wang, H., Chen, H.X., Wu, C.M., 2013. Metamorphic P-T-t paths retrieved from the amphibolites, Lushan terrane, Henan Province and reappraisal of the Paleoproterozoic tectonic evolution of the Trans-North China Orogen. Precambr. Res. 238, 61–77.
Lu, J.S., Wang, G.D., Wang, H., Chen, H.X., Wu, C.M., 2014. Palaeoproterozoic metamorphic evolution and geochronology of the Wugang block, southeastern terminal of the Trans-North China Orogen. Precambr. Res. 251, 197–211.
Maliva, R.G., Knoll, A.H., Simonson, B.M., 2005. Secular change in the Precambrian silica cycle: insights from chert petrology. Geol. Soc. Am. Bull. 117, 835–845.
Meinert, L.D., Dipple, G.M., Nicolescu, S., 2005. World skarn deposits. Economic Geology 100th Anniversary Volume, 299–336.
Mloszewska, A.M., Pecoits, E., Cates, N.L., Mojzsis, S.J., O'Neil, J., Robbins, L.J., Konhauser, K.O., 2012. The composition of Earth's oldest iron formations: The Nuvvuagittuq Supracrustal Belt (Québec, Canada). Earth Planet. Sci. Lett. 317–318, 331–342.
Mollo, S., Putirka, K., Iezzi, G., Scarlato, P., 2013. The control of cooling rate on titanomagnetite composition: implications for a geospeedometry model applicable to alkaline rocks from Mt. Etna volcano. Contrib. Miner. Petrol. 165, 457–475.
Mueller, R.F., 1967. Mobility of the elements in metamorphism. J. Geol. 75, 565–582.
Nadoll, P., Mauk, J.L., Hayes, T.S., Koenig, A.E., Box, S.E., 2012. Geochemistry of magnetite from hydrothermal ore deposits and host rocks of the Mesoproterozoic Belt Supergroup, United States. Econ. Geol. 107, 1275–1292.
Nadoll, P., Angerer, T., Mauk, J.L., French, D., Walshe, J., 2014. The chemistry of hydrothermal magnetite: a review. Ore Geol. Rev. 61, 1–32.
Nielsen, R.L., Forsythe, L.M., Gallahan, W.E., Fisk, M.R., 1994. Major- and trace-element magnetite-melt equilibria. Chem. Geol. 117, 167–191.
Ohmoto, H., 2003. Nonredox transformations of magnetite-hematite in hydrothermal systems. Econ. Geol. 98, 157–161.
Pearce, N.J.G., Perkins, W.T., Westgate, J.A., Gorton, M.P., Jackson, S.E., Neal, C.R., Chenery, S.P., 1997. A compilation of new and published major and trace element data for NIST SRM 610 and NIST SRM 612 Glass Reference Materials. Geostandards Newsletter 21, 115–144.
Pecoits, E., Gingras, M.K., Barley, M.E., Kappler, A., Posth, N.R., Konhauser, K.O., 2009. Petrography and geochemistry of the Dales Gorge banded iron formation: paragenetic sequence, source and implications for palaeo-ocean chemistry. Precambr. Res. 172, 163–187.
Planavsky, N., Scott, C., Gill, B.C., Bekker, A., Lyons, T.W., 2010. Tracking Zn bioavailabilty through time: New insights from sulfidic black shales. American Geophysical Union, Fall Meeting 2010, abstract id. OS33E-1510.
Qi, R.Z., 1987. Genesis of BIF of the Precambrian Huoqiu Group. Bulletin of Nanjing Institute of Geology, Chinese Academy of Geological Sciences, pp. 1–20.
Qi, R.Z., Yao, G.Y., 1982. The metamorphism of Huoqiu Group. Bulletin of Nanjing Institute of Geology, Chinese Academy of Geological Sciences, pp. 30–46.
Ray, G.E., Webster, I.C.L., 2007. Geology and chemistry of the low Ti magnetite-bearing Heff Cu-Au skarn and its associated plutonic rocks, Heffley Lake, South-Central British Columbia. Exploration Mining Geol. 16, 159–186.
Reguir, E.P., Chakhmouradian, A.R., Halden, N.M., Yang, P., 2008. Early magmatic and reaction-induced trends in magnetite from the carbonatites of Kerimasi, Tanzania. Can. Mineral. 46, 879–900.
Righter, K., Sutton, S.R., Newville, M., Le, L., Schwandt, C.S., Uchida, H., Lavina, B., Downs, R.T., 2006. An experimental study of the oxidation state of vanadium in spinel and basaltic melt with implications for the origin of planetary basalt. Am. Mineral. 91, 1643–1656.
Rosière, C.A., Rios, F.J., 2004. The origin of hematite in high-grade iron ores based on infrared microscopy and fluid inclusion studies: the example of the Conceição mine, Quadrilátero Ferrífero, Brazil. Econ. Geol. 99, 611–624.
Rusk, B., Oliver, N.H.S., Cleverley, J.S., Blenkinsop, T.G., Zhang, D.X., Williams, P., Habermann, P., 2010. Physical and chemical characteristics of the Ernest Henry iron oxide copper gold deposit, Australia; implications for IOGC genesis. In: Porter, T.M. (Ed.), Hydrothermal Iron Oxide Copper-Gold and Related Deposits: A Global Perspective. Pgc Publishing, Adelaide, pp. 201–218.
Ryabchikov, I.D., Kogarko, L.N., 2006. Magnetite compositions and oxygen fugacities of the Khibina magmatic system. Lithos 91, 35–45.
Saito, M.A., Sigman, D.M., Morel, F.M.M., 2003. The bioinorganic chemistry of the ancient ocean: the co-evolution of cyanobacterial metal requirements and biogeochemical cycles at the Archean-Proterozoic boundary? Inorg. Chim. Acta 356, 308–318.
Santosh, M., Sajeev, K., Li, J.H., Liu, S.J., Itaya, T., 2009. Counterclockwise exhumation of a hot orogen: the Paleoproterozoic ultrahigh-temperature granulites in the North China Craton. Lithos 110 (1–4), 140–152.
Shen, F.N., 1994. The discovery of unconformity within the Taihua Group and definition of its stratigraphic sequence in the Lushan area, Henan. Regional Geol. China 2, 135–140 (in Chinese with English abstract).
Sillitoe, R.H., 2010. Porphyry copper systems. Econ. Geol. 105, 3–41.
Skublov, S., Drugova, G., 2003. Patterns of trace-element distribution in calcic amphiboles as a function of metamorphic grade. Can. Mineral. 41, 383–392.
Toplis, M.J., Carroll, M.R., 1995. An experimental study of the influence of oxygen fugacity on Fe-Ti oxide stability, phase relations, and mineral-melt equilibria in ferrobasaltic systems. J. Petrol. 36, 1137–1170.
Toplis, M.J., Corgne, A., 2002. An experimental study of element partitioning between magnetite, clinopyroxene and iron-bearing silicate liquids with particular emphasis on vanadium. Contrib. Miner. Petrol. 144, 22–37.
Tu, Y.J., 1998. Geochemical comparing of two types of amphibolites within the Taihua Group in Lushan County, Henan Province and their tectonic settings. Geochimica 27, 412–421.
Tu, X.L., Zhang, H., Deng, W.F., Ling, M.X., Liang, H.Y., Liu, Y., Sun, W.D., 2011. Application of RESOlution in situ laser ablation ICP-MS in trace element analyses. Geochimica 10, 83–98 (in Chinese with English abstract).
Van Baalen, M.R., 1993. Titanium mobility in metamorphic systems: a review. Chem. Geol. 110, 233–249.
Wan, Y.S., Wilde, S.A., Liu, D.Y., Yang, C.X., Song, B., Yin, X.Y., 2006. Further evidence for ~1.85 Ga metamorphism in the Central Zone of the North China Craton: SHRIMP U-Pb dating of zircon from metamorphic rocks in the Lushan area, Henan Province. Gondwana Res. 9 (1–2), 189–197.
Wan, Y.S., Liu, D.Y., Wang, S.Y., Zhao, X., Dong, C.Y., Zhou, H.Y., Yin, X.Y., Yang, C.X., Gao, L.Z., 2009. Early Precambrian crustal evolution in the Dengfeng area, Henan Province (eastern China): constraints from geochemistry and SHRIMP U-Pb zircon dating. Acta Geol. Sin. 83 (7), 982–999 (in Chinese with English abstract).
Wan, Y.S., Dong, C.Y., Wang, W., Xie, H.Q., Liu, D.Y., 2010. Archaean basement and a Palaeoproterozoic collision orogen in the Huoqiu area at the southeastern margin of the North China Craton: evidence from SHRIMP U-Pb zircon geochronology. Acta Geol. Sin. 84, 91–104.
Wechsler, B.A., Lindsley, D.H., Prewitt, C.T., 1984. Crystal-structure and cation distribution in titanomagnetites ($Fe_{3-x}Ti_xO_4$). Am. Mineral. 69, 754–770.
WUSTEEL, 2003. Verification report on resources of the Tieshan iron deposit in the Wuyang area, Henan province (internal data) (in Chinese).
Xue, L.W., Yuan, Z.L., Zhang, Y.S., Qiang, L.Z., 1995. The Sm-Nd isotope ages of Tai-hua Group in the Lushan area and their implications. Geochimica 24, 92–97 (in Chinese with English abstract).
Yang, C.X., 2008. Zircon SHRIMP U-Pb ages, geochemical characteristics and environmental evolution of the Early Precambrian metamorphic series in the Lushan area, Henan, China. Geol. Bull. China 27 (4), 517–5333 (in Chinese with English Abstract).
Yang, X.Y., Wang, B.H., Du, Z.B., Wang, Q.C., Wang, Y.X., Tu, Z.B., Zhang, W.L., Sun, W.D., 2012. On the metamorphism of the Huoqiu Group, forming ages and mechanism of BIF and iron deposit in the Huoqiu region, southern margin of North China carton. Acta Petrol. Sin. 28 (11), 3476–3496 (in Chinese with English abstract).
Yu, S.J., Liang, Y.H., Du, S.H., Li, S.Z., Liu, K.J., 1981. Research in ore-forming geological characteristic and configuration of iron-bearing basin of Tieshanmiao-type iron deposits of Late Archaean in the central Henan and western Anhui. J. Yichang Inst. Geol. Mineral Resour., Chin. Academy Geol. Sci. 3, 68–83 (in Chinese with English abstract).
Yu, S.J., Li, Z.S., Liu, K.J., Zhuang, L.C., Li, Z.C., 1982. A preliminary study on the mineralogy of the Zhaoanzhuang-type iron-ore deposit, Wuyang, Henan province. J. Yichang Inst. Geol. Mineral Resour., Chinese Acad. Geol. Sci. 5, 1–24 (in Chinese with English abstract).
Yu, S.J., Zhuang, L.C., Li, Z.S., Li, Z.C., Liu, K.J., 1983. Genesis and minerogenetic characteristics of the iron deposit of Zhaoanzhuang type in the Wuyang region, Henan province. Geochemica 1, 71–80.
Zhai, M.G., Guo, J.H., Liu, W.J., 2005. Neoarchean to Paleoproterozoic continental evolution and tectonic history of the North China Craton: a review. J. Asian Earth Sci. 24 (5), 547–561.
Zhai, M.G., Liu, W.J., 2003. Palaeoproterozoic tectonic history of the North China craton: a review. Precambr. Res. 122 (1–4), 183–199.
Zhai, M.G., Santosh, M., 2011. The early Precambrian odyssey of the North China Craton:

a synoptic overview. Gondwana Res. 20 (1), 6–25.
Zhang, G.W., Bai, Y.B., Sun, Y., 1985. Composition and evolution of the Archean crust in central Henan, China. Precambr. Res. 27 (1–3), 7–35.
Zhang, L.C., Zhai, M.G., Wan, Y.S., Guo, J.H., Dai, Y.P., Wang, C.L., Liu, L., 2012. Study of the Precambrian BIF-iron deposits in the North China Craton: progresses and questions. Acta Petrol. Sin. 28 (11), 3431–3445 (in Chinese with English abstract).
Zhao, G.C., Wilde, S.A., Cawood, P.A., Sun, M., 2001. Archean blocks and their boundaries in the North China Craton: Lithological, geochemical, structural and P-T path constraints and tectonic evolution. Precambr. Res. 107 (1), 45–53.
Zhao, G.C., Sun, M., Wilde, S.A., Li, S.Z., 2005. Late Archean to Paleoproterozoic evolution of the North China Craton: key issues revisited. Precambr. Res. 136 (2), 177–202.
Zhou, Y.Y., Zhao, T.P., Xue, L.W., Wang, S.Y., 2009. Geochemistry and origin of Neoarchean amphibolites in Songshan, Henan province. Acta Petrol. Sin. 25, 3043–3056 (in Chinese with English abstract).